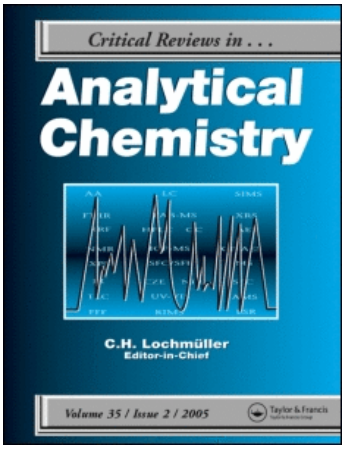

Critical Reviews in Analytical Chemistry
Publication details, including instructions for authors and subscription information:
http://www.informaworld.com/smpp/title~content=t713400837

Recent Advances in Pulse Cyclic and Square-Wave Cyclic Voltammetric Analysis

Gordon N. Eccles[a]
[a] ICI Explosives Canada, Technical Centre, Quebec, Canada

To cite this Article Eccles, Gordon N.(1991) 'Recent Advances in Pulse Cyclic and Square-Wave Cyclic Voltammetric Analysis', Critical Reviews in Analytical Chemistry, 22: 5, 345 — 380
To link to this Article: DOI: 10.1080/10408349108051639
URL: http://dx.doi.org/10.1080/10408349108051639

Critical Reviews in Analytical Chemistry, 22(5):345–380 (1991)

Recent Advances in Pulse Cyclic and Square-Wave Cyclic Voltammetric Analysis

Gordon N. Eccles, Ph.D.

ICI Explosives Canada, Technical Centre, 801 Richelieu Blvd., McMasterville, Quebec, Canada J3G 1T9

ABSTRACT: If rapid quantitative electrochemical analysis was to evolve, the charging current that plagues electrochemical measurements had to be minimized. These currents occur when rapidly changing potentials are applied to an electrode solution interface. This initiated the research of modified potential waveforms such as those used in pulse and square wave polarography. These methods have been shown to filter out much of the effect of charging current and are used extensively in routine analysis. Similarly, pulse methods coupled with cyclic voltammetry also reduce noise and analysis times and in addition provide more qualitative information. A historical review of the various techniques that reject charging current is discussed with emphasis placed on recent studies with modified cyclic voltammetry waveforms.

KEY WORDS: square-wave, cyclic voltammetry, pulse cyclic voltammetry, square-wave cyclic voltammetry, linear sweep.

I. GENERAL OVERVIEW OF CYCLIC VOLTAMMETRY AND CHARGING CURRENT

Cyclic voltrammetry (CV) has become a powerful and versatile technique in determining analytical information from electroactive compounds in solution, and its fundamental characteristics have been examined (e.g., References 1 to 3). Using this technique, the electrochemical reversibility of electron transfer processes may be conveniently studied, and characteristics such as reduction potentials, formation constants, rate constants, and reaction stoichiometry may often be rapidly evaluated. However, care must be exercised when reviewing the resultant data since misinterpretations can occur if the user is unaware of the limitations of the technique.[4-7] Diagnostic information has been obtained from studies of the chemistry ocurring at the surfaces of mercury and solid (carbon) electrodes in static solutions.[1,8] Inorganic chemists have used CV to evaluate ligand effects on Ru-Ru complexes and multinuclear clusters for reversibility and oxidation/reduction potential shifts.[9] Rice and Spence[10] studied the properties of new molybdenum (IV) complexes using CV. In organic electrochemistry, Bobbitt and Willis utilized CV to study the mechanisms of some biosynthetic reaction pathways,[11] and Nelson et al.[12] monitored electrochemically generated free radicals.

A. General Principles of Cyclic Voltammetry

In CV electron transfer occurs at or near an electrode surface when the energetics of the system favors either a reduction (electrode to solution) or an oxidation (solution to electrode) process. The net flow of electrons (response) is measured against time as current. The energy applied at the electrode is a voltage waveform containing both positive and negative scan segments. The initial segment is determined by the species in the bulk solution. For example, if the

1040-8347/91/$.50

analyte is in its fully oxidized form, then the initial scan segment would necessarily be toward a more negative potential. The first example of CV, according to Adams,[1] was given by Sevcik[13] in 1948. A classic theoretical treatment of stationary electrode voltammetry for single scan and cyclic methods applied to reversible, irreversible, and kinetic systems has been presented by Nicholson and Shain.[4,5]

The voltage scan rate in CV is variable, allowing selected electrochemical reactions to occur. For example, if the electrochemical species formed at an electrode at slow voltage scan rates reacts irreversibly with another component in the solution matrix, then on the reverse scan no current response is observed. However, by increasing the scan rate to the point where the irreversible coupled chemical reaction is not able to occur (i.e., short resident time of the generated electroactive species), a reverse-response current may be observed. The advantages of rapid-scan CV have been realized for many years, and oscillographic methods have been developed[8,14] for this purpose which follow the fundamental equations developed by Heyrovsky.[15] For example, the properties of transient intermediates were studied some time ago by Kemula and Kublik.[8] Although oscillographic methods have been used, they are not practical due to their limited resolution.

The flexibility of the CV waveform makes it popular among electrochemists. Most importantly, a range of desired potentials limited only by the degradation of the solvent or the electrode (e.g., Hg at positive potentials) may be scanned. The only serious limitation is that, at higher scan rates, the current due to charging of the double layer becomes so significant that Faradaic currents are completely dominated. Pulse techniques, such as differential-pulse voltammetry or square-wave voltammetry, are known to filter charging currents at higher scan rates; therefore, it seems plausible that coupling a pulse method with CV might offer the same benefit. The next sections of the report discuss the Faradaic and charging-current components, following which, an historical review of various pulse methods is presented.

B. Randles-Sevcik Equation and Double-Layer Charging Current

Consider the Randles-Sevcik equation for the voltammetric peak current of a reversible system at 25°C,[7]

$$i_P = (2.69 \times 10^5)n^{3/2}AD_o^{1/2}\nu^{1/2}C_o^* \qquad (1)$$

where i_p is the peak current, n is the electron stoichiometry, A is the electrode area, D_o is the diffusion coefficient, ν is the scan rate, and C_o^* is the bulk concentration of the electroactive species. This relationship indicates a dependence of the current response on the square root of the scan rate. Another component of the measured response current is the current due to charging the electrode to a given potential, as described by the following equation[7]

$$i_c = C\frac{dE}{dt} = AC_{dl}\nu \qquad (2)$$

where i_c is the charging current, A is the electrode area, C_{dl} is the differential capacitance of the double layer per unit area, and ν is the scan rate. Equations 1 and 2 indicate that, at high scan rates, the charging current will become a significant component of the response signal. This feature is compounded by the fact that C_{dl} is a function of potential, and the dependence is not necessarily linear (first observed by Grahame[16] with mercury). To eliminate the existence of i_c is fundamentally not possible, but many novel methods have been developed to effectively filter out charging current.

II. CHARGING-CURRENT DISCRIMINATION TECHNIQUES

This section covers various aspects of pulse techniques that have been used to discriminate against charging current. Alternating-current techniques have a wide range of instrumental approaches in minimizing charging-current effects[17,18] and are not discussed here. The wave-

forms suggested by Barker[19-22] have paved the way for others and deserve special attention here.

A. Barker Waveforms

Square-wave voltammetry, introduced by Barker and Jenkins,[19] can be used to alleviate the undesirable effect of the double-layer capacitance current on the sensitivity of an alternating current (AC) polarographic analyzer. A square-wave voltage is substituted for the usual sinusoidal polarizing voltage, and the amplitude of the AC component of the cell current is measured shortly before each transition in the applied voltage. Preliminary results reported by these workers suggested that the method could be useful for the detection of reversibly reduced metallic ions at concentrations down to 2×10^{-7} *M*. An extension of the method, subsequently known as electrochemical stripping analysis, permitted the detection of certain metallic ions at concentrations of 10^{-9} *M*, offering the lowest detection limit of any commonly used electroanalytical technique.[23] It is interesting to note that Barker and Jenkins doubted the utility of methods that provided higher sensitivity, due to the poor quality of reagents at that time.

Some of the general principles of square-wave voltammetry are illustrated in Figure 1. Briefly, if a square-wave voltage (Figure 1a) is oscillating above and below (50 mV in each direction) the half-wave potential of a one-electron reversible species in solution, then during each pulse the current flowing is nearly limiting. During the application of each pulse, only two events occurring at or near the working electrode (a double-layer charging-current response; i_c, Equation 2), and an oxidation- or reduction-current response (i_p Equation 1), the double-layer charging current begins to decay after a pulse transition in a fashion similar to an electronic capacitor (Figure 1b) with the decay curve reaching a minimum current condition near the end of the pulse (n.b., long pulses [e.g., greater than about 200 ms] would result in $i_c = 0$). Finally, Faradaic current (shown in Figure 1c) increases to almost limiting-current conditions and, similarly, a decay occurs during the lifetime of the pulse. The rate of decay is described by diffusion-limited current equations in chronoamperometry.[24] The Faradaic current decays at a slower rate during a pulse compared with that of the double-layer capacitative-current decay, and consequently, if the current is measured near the end of each pulse, it should be due mainly to a Faradaic process. This has effectively filtered out the charging-current component, providing only the desired response. The description outlined above is based on a polarizing voltage resting on a theoretical half-wave potential. This theoretical potential is that at which the current is equal to $i_d/2$, as in the relationship

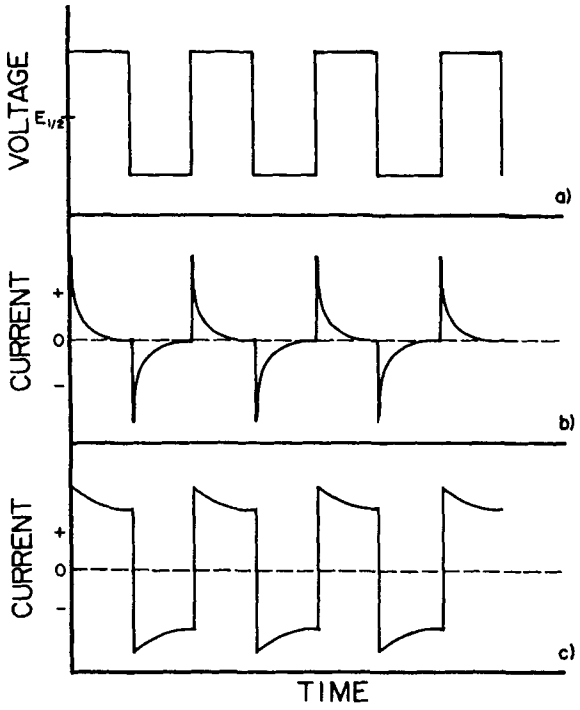

FIGURE 1. Voltage and current waveforms. (a) voltage vs. time; (b) charging current decay vs. time curve; (c) faradaic current decay vs. time curve.

$$E = E_{1/2} - \frac{0.059}{n} \log \frac{i}{i_d - i} \qquad (3)$$

where E and n have their usual meaning, i_d is the diffusion-limited current, and i is the current response obtained at nonlimiting potentials. Naturally, for situations involving unknown species, $E_{1/2}$ is rarely known and must be determined experimentally. In the case of square-wave voltam-

metry, a square wave is superimposed on a slowly changing ramp, and an alternating current is obtained as $E_{1/2}$ is approached. The difference current obtained during each half-cycle is plotted against the potential, the term for this type of data presentation being known as derivative voltammetry. It should be noted that the observed peak potential (E_p) is not equal to the half-wave potential ($E_{1/2}$). The difference between E_p and $E_{1/2}$ is dependent upon the excitation technique employed and can only be predicted for reversible couples.

1. Pulse Polarography

Barker, working with Jenkins, constructed such a square-wave device in 1952 and later, in 1960 with collaboration with Gardner,[21] developed pulse polarography. Pulse polarography provided enhanced sensitivities for reversibly reduced and irreversibly reduced ions at concentrations down to about 10^{-8} and 5×10^{-8} *M*, respectively. This technique preceded further development of the square-wave technique due to design difficulties in reducing the square-wave frequency from 225 Hz (initial square-wave device) to 10 Hz. Two modes of operation were described. The first of these was normal pulse polarography in which the pulses varied in amplitude (which was proportional to the elapsed time from the start of the sweep) from 0 to 1 V. In the second method, the 50-mV pulses (on a slowly changing polarizing voltage) occur approximately 2 s after the fall of the preceding mercury drop, and have a duration of 40 ms. As with square-wave polarography, data are acquired prior to each voltage transition, and a derivative polarogram is obtained.

The theory of the diffusion equation in pulse polarography and the problem of kinetic (including catalytic) processes were investigated by Brinkman and Los.[25-27] The differential-pulse polarographic technique virtually eliminates charging current (except for a small DC component), and therefore both high Faradaic-to-charging current ratios and high sensitivity have been achieved, as reported by Osteryoung and other workers.[28-30] Alternate drop-pulse polarography, in which measurement times occur at identical drop areas, completely compensates the capacitative background due to drop expansion.[31] A hybrid of differential-pulse and normal-pulse waveforms retains all of the advantages of normal-pulse polarography, and was suggested for use in the study of reactions at solid electrodes and in cases of electrode passivation or filming.[32] Pulse voltammetry at a rotated electrode[33] and fast-sweep differential-pulse voltammetry at a dropping mercury electrode[34] illustrate extensions of the Barker technique. A review of the theory and application of pulse polarography (108 references) was prepared by Osteryoung and Hasebe.[35]

2. Stripping Voltammetry

Others methods of obtaining increased sensitivity include the use of a sessile mercury drop (developed by Barker[20]) and the hanging mercury drop (developed and evaluated by Kemula and Kublik[36]). These methods involved polarizing a mercury drop at a potential that would reduce metallic ions such that they became concentrated in the drop. Following this, a positive potential scan was performed and the resulting oxidation current was monitored. This technique is used in electrochemical stripping analysis, for which a number of methods have been developed (see review by Kissinger and Heineman[23] and references therein). In addition, theoretical treatment of staircase voltammetric stripping from the thin-film mercury electrode has been indicated as an alternative to both differential-pulse and linear-scan voltammetric stripping analysis.[37]

3. Radio-Frequency and Square-Wave Intermodulation Voltammetry

An evaluation of the capabilities of these two techniques by Barker and co-workers[20,22] indicated that they can be easily adapted to very small cell volume (0.01 ml) systems. The radio-frequency (RF) technique is a useful detection method for reversible and irreversible compounds, while the square-wave intermodulation method has higher sensitivities for quasireversible reactions.

The RF technique, when employing frequencies between 100 kHz and 6.4 MHz and an amplitude of less than 10 mV, creates Faradaic rectification. Oldham[38] discussed the theory and application of this technique to the Hg_2^{2+}/Hg electrode. This effect can be used to study the kinetics of very rapid electrode processes and has been used to determine transfer coefficients and heterogeneous rate constants for certain metallic ions. The RF method has been utilized in analytical work by increasing the amplitude to 25 mV (to obtain higher sensitivities) at 400 kHz. Higher frequencies would cause RF heating of the solution. As mentioned above, Barker was able to adapt the technique to microcells and obtained RF polarograms of metallic ions, with well-defined peaks at quantities down to 10^{-10} g in solutions as small as 0.01 ml.

The intermodulation technique involves modulating the frequency in contrast to the amplitude, and its principal merits are that reversible and wholly irreversible reactions are unaffected by frequency changes and that quasireversible reactions having different heterogeneous rate constants may be studied.

Barker et al.[22] earlier suggested the most valuable of the available modes of electroanalytical voltammetric techniques to be (1) square-wave; (2) radio-frequency; (3) square-wave intermodulation; and (4) linear scan. They also mentioned that pulse-voltammetry provided a higher sensitivity, but it often cannot compete with a fully developed square-wave polarograph. Pulse voltammetry was also reported as inferior to RF voltammetry regarding sensitivity and speed of data acquisition. Unfortunately, the development and refinement of techniques 2 and 3 were impeded by instrumentation limitations, and further investigations of these two techniques may be beneficial.

B. Square-Wave Voltammetry (Ramaley and Osteryoung Waveforms)

Osteryoung and various co-workers have rigorously evaluated pulse voltammetry by examining a variety of excitation waveforms, such as alternative drop voltammetry, to reduce capacitative effects and/or compensate for the different drop sizes at different measurement times. Recent attention has been given to what they have termed square-wave voltammetry.[39-42] Krause and Ramaley[43] earlier developed the theory for the hanging mercury drop electrode; however, the treatment was limited to small step heights (and consequently, slow scan rates). A brief description of the square-wave voltammetry waveform follows, using the nomenclature of Christie et al.[39,44]

Referring to Figure 2, the basic time unit τ corresponds to the step width in staircase voltammetry, and ΔE is the step height. For the square-wave form, E_{sw} corresponds to the magnitude of each of the two potential pulses with respect to the staircase potential. The fraction of each period during which the potential is high is σ; hence, the length of the forward pulse is $\sigma\tau$. The current is measured twice during each staircase period: at time $p_1\tau$ during the forward pulse, and at time $p_2\tau$ during the reverse pulse. The coefficients p_1, p_2, and σ are all fractions less than unity, and $p_1 < \sigma < p_2$. It can be seen that a symmetric square-wave occurs when $\sigma = 0.5$ and $p_1 = p_2 - \sigma$.

In Osteryoung square-wave voltammetry, a symmetric waveform is applied and a complete voltage range is scanned during the life of one drop (a few seconds). A current measurement is made during the forward-going pulse ($p_1\tau$), and a second current measurement is made during the reverse pulse ($p_2\tau$). The difference current is obtained and sent to an appropriate displaying device. A distinct advantage of this technique is

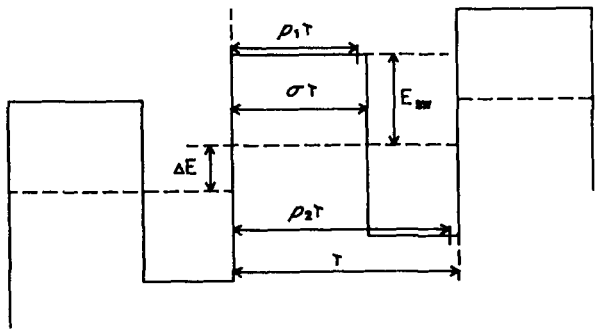

FIGURE 2. Square-wave waveform and parameters. ΔE = step height. τ = step width. Coefficients p_1, σ, p_2 are all fractions less than unity and $p_1 < \sigma < p_2$. E_{sw} = square wave amplitude.

that the forward- and reverse-pulse currents may be plotted individually.[39]

In a comprehensive treatment, Christie and Osteryoung[39] developed the theory of square-wave voltammetry at the dropping mercury electrode. Subsequently, Turner et al.[40] experimentally verified the earlier theoretical work and found excellent agreement. This technique was shown to have the same order of sensitivity (e.g., the detection limit for cadmium in 0.1 HCl was found to be 7×10^{-8} *M*) as differential pulse polarography, but was much faster to perform.

C. Pulse and Square-Wave Cyclic Voltammetry

One of the first works to describe the utility of combining a pulse method with cyclic voltammetry was that by Drake et al.,[45] who presented a number of experimental examples illustrating the salient features of this technique. For example, 9,10-diphenylanthracene (DPA) could be oxidized and reduced at a platinum electrode in acetonitrile, and a staircase voltammograms could be recorded in the presence of the pulse. Hence, two voltammograms could be obtained during a single experimental run (one from the applied staircase time domain; one from the pulse time domain). The pulse duration was 200 μs compared with a step time of 1 ms. The pure pulse curve was experimentally shown to be independent of scan rate, and the apparent distortion and scan rate dependence in the differential pulse results at fast scan rates is entirely due to the direct current terms. This work showed that important additional information can be obtained with this dual time-domain technique, concerning both the nature of the technique and the electrode process under consideration. They termed this method cyclic differential-pulse voltammetry. Choosing which of the two techniques, CV or differential-pulse voltammetry, precedes the other in the combined name is a matter of choice. One could consider that it is CV that has been modified using a pulse method, and adopt the term pulse cyclic voltammetry (PCV) for pulse trains (symmetric or not) that are added to a linearly changing ramp, and adopt the term square-wave cyclic voltammetry (SWCV) for pulse trains (symmetric or not) that are added to a staircase ramp. These waveforms are discussed further below.

Okamoto[46] derived a theory for single-drop square-wave voltammetry which was limited to less than a 10-mV square wave, superimposed on a triangular sweep. The experimental results agreed better with theory for the forward sweep than for the reverse sweep. An improvement in the limit of detection was obtained by Gajda and Horák[47] when they applied a square wave superimposed on a linear changing ramp. The low detection limits were obtained using long, dropping mercury electrode drop times in the order of 100 s. These investigators used sweep reversal, but did not study the effects.

Ramaley and Tan[48] contributed to the development of the theory for cyclic single-drop square-wave voltammetry by considering the influence of electrode sphericity. Their theory was verified with Fe (III)/(II) and Cd (II)/Cd·Hg systems using a dropping mercury electrode. An expanding sphere treatment obtained by adding a spherical correction to the expanding plane theory gave the best fit to the experimental data. In addition, the forming amalgam fit the simple theory to a lesser extent that other reactions, especially on the reverse sweep.

Eccles and Purdy[49] developed a microprocessor-controlled PCV instrument. PCV voltammograms of ferricyanide showed that linear calibration curves were obtained for both the forward- and reverse-scan differential current peaks, and were superimposable, indicating the expected reversibility of the couple. In studies with static and flowing solutions, the same authors[50,51] showed an enhancement in sensitivity when using PCV, compared to conventional CV. They were able to obtain additional information about the electrode processes, and, in the specific case of the quinone/hydroquinone couple, it was shown that an improved sensitivity is attained for the oxidation process during the reverse scan in flow injection analysis (FIA). These studies indicated that, with a PCV detector, better analytical data can sometimes be found in the reverse scan. The flow cell waste may in fact contain the most valuable information.

Other than the work described above, very little has been published on PCV or SWCV. Nonetheless, it is argued that these techniques

have much to offer in studying electrochemical processes. One feature of these techniques is the increased speed with which a CV run may be obtained, suggesting the advantage of their use in electrode kinetics studies. The dual time domain offers another advantage of kinetic studies. Used as a rapid-scan detector in flowing streams, another dimension is added: the possibility of performing both qualitative and quantitative analysis.

The following section discusses various ways of adding pulse methods to a CV triangular waveform, and discusses the effects of these waveforms on the charging-current decay curves at various electrodes.

III. GENERAL PRINCIPLES OF PULSE CYCLIC AND SQUARE-WAVE CYCLIC VOLTAMMETRY

A. Excitation Waveforms

In the previous section, various types of excitation waveforms were discussed, noting that some confusion may exist in the nomenclature. This author has adopted the terminology used by Christie et al.[39] (as shown in Figure 2). The waveforms that are considered here are based on the triangular-shaped signal used in CV. By combining this signal with pulse methods, a variety of modified CV waveforms are possible. Of these, only four are considered herein (illustrated in Figure 3).

At first glance (Figure 3), the general triangular wave shape in all four waveforms appears similar to that used in CV; however, each possesses a pulse method variation. The waveforms depicted in Figures 3a and b are derived by the addition of a square-wave pulse train to a triangular wave and are offset by π, relative to each other. They are termed pulse CV (PCV) excitation signals. The waveforms in Figures 3c and d are termed square-wave cyclic voltammetry (SWCV) and are also out of phase by π, relative to each other. These differences may be more obvious, comparing the direction of the first pulse with respect to the direction of the linear ramp.

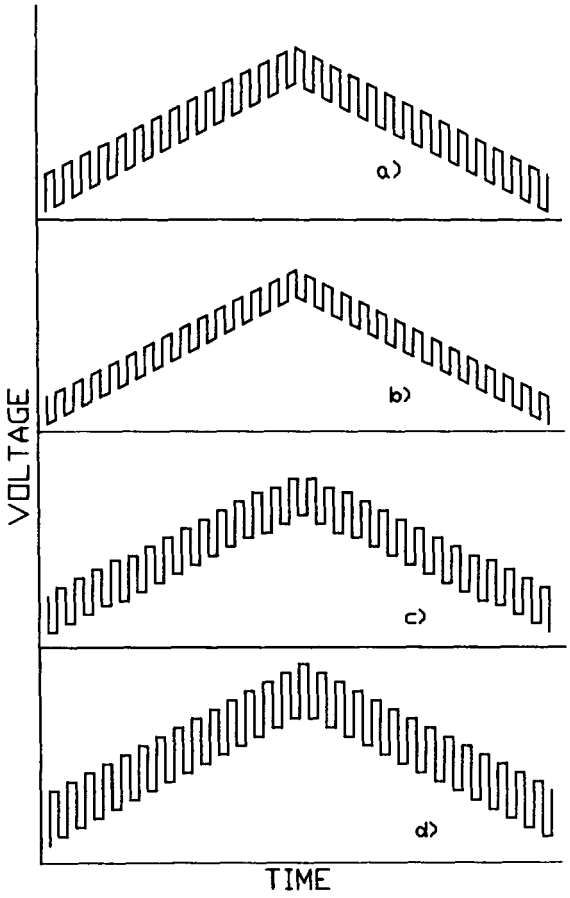

FIGURE 3. PVC (a and b) and SWCV (c and d) waveforms.

In Figure 3a and d, the pulse direction follows the direction of the ramp; Figure 3b and c, the pulse and ramp are out of phase. The major difference between the two excitation signals in Figures 3a and b and the two signals in figures 3c and d is that the potential continues to ramp during the lifetime of a pulse in the former cases. The forward scan is equal in all respects to the linear-sweep pulse method (discussed earlier). The reverse scan (or the mirror image of the forward scan) is also equivalent to a linear-sweep pulse method. The mating of the two halves establishes a modified cyclic voltammetric waveform, and forms the basis of PCV and SWCV. Note that only symmetric square waves (σ = 0.5) are shown, and the voltage axis can be labeled as increasing positive or negative in magnitude, depending on the forward scan direction.

1. Pulse Periods and Associated Current Response Curves

The initial pulse periods for the forward scans in each waveform of Figure 3 are shown in figure 4. The waveform in Figure 4a is attributed to Barker and Jenkins;[19] that in Figure 4c to Krause and Ramaley;[43] and that in Figure 4d, to Christie et al.[39] The waveform in Figure 4b is an interesting variation of that in Figure 4a, which has not been discussed in the literature and is considered later. The parameters for the waveforms in Figures 4a, c, and d have been discussed previously. The current-response curves below each pulse period represent the shape and direction of a typical charging-current decay curve. The relationship describing the charging of an electronic capacitor, used to describe the electrode solution double layer charging current, may be given as

$$i = \frac{V}{R} e^{-t/RC} \qquad (4)$$

where i is the current, V is the applied voltage, R is the resistance, C is the capacitance, and t is the time in seconds.

One should note in comparing the decayed curves in Figure 4, that τ and ΔE are equal in all four waveforms (i.e., the pulse frequencies and voltage ramps are identical). In addition, the measurement times and the voltage at which the measurements are taken are identical for the different waveforms, as indicated by the tick mark locations. Thus, the Faradaic current is measured at the same potential regardless of which waveform is implemented. Examining Figure 4, it is evident that the course in which the waveforms approach the measuring voltages vary in each case. This is discussed further below, considering the PCV waveforms first, and then the SWCV waveforms.

One should first compare the PCV waveforms (Figure 4a and b). The contribution to the background from the linearly changing ramp during the lifetime of a pulse will not be discussed at this stage. If one considers that the upward

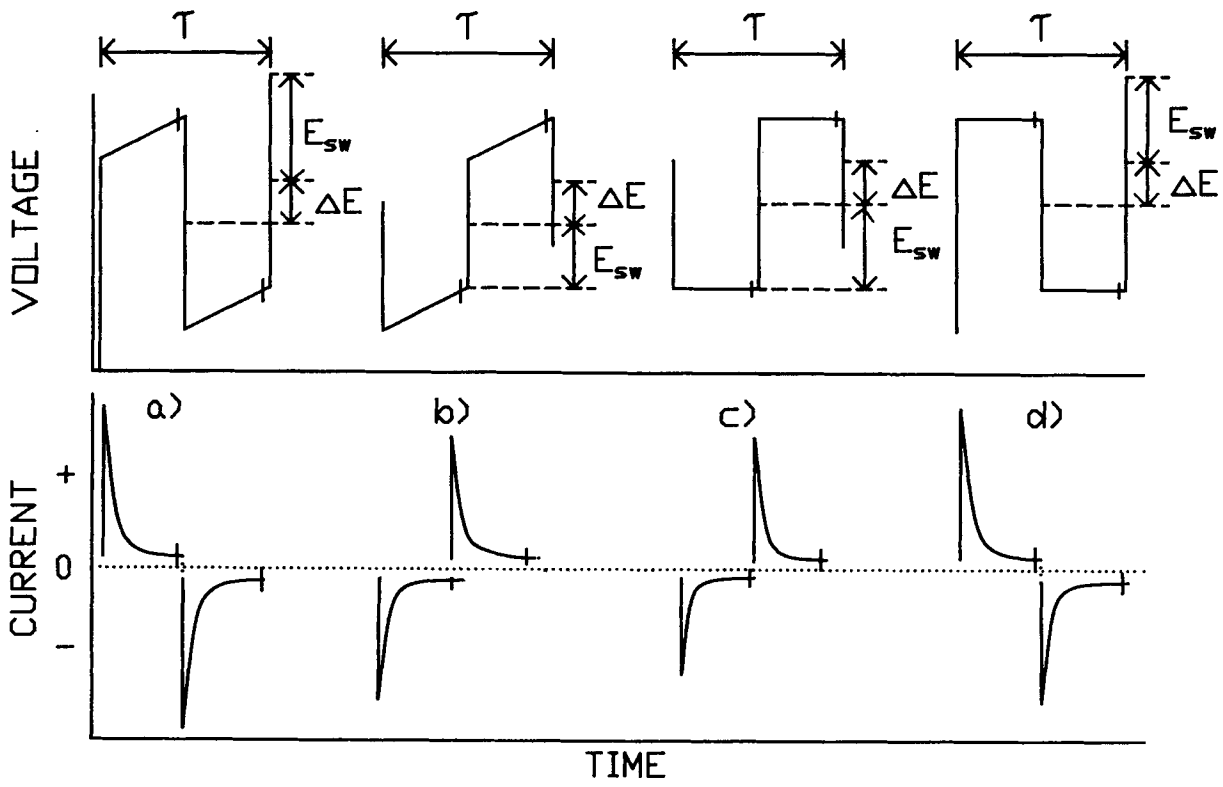

FIGURE 4. PCV and SWCV waveform periods and the current relationships.

pulses (in phase with the ramp) are forward pulses, and that the downward pulses (out of phase with the ramp) are reverse pulses, than the first pulse in Figure 4a is a forward pulse, and the first pulse in Figure 4b is a reverse pulse. The forward-pulse currents are measured at equal voltage positions at different times; the same is true for the reverse-pulse currents. Figure 4 shows the charging-current decay curves in b to be smaller in magnitude than in a. This is shown to be the case by applying Equation 4, where R = 200 Ω[52] and C = 100 μF[53] for a carbon electrode: hence, the forward-pulse transition for case 4a is 0.110 V, and the forward-pulse transition for case 4b is 0.090 V (n.b., the pulse-transition values were obtained by a graphical method, where all four waveforms were drawn with E_{sw} set to 0.050 V). These are plotted in Figure 5 for the forward PCV pulses depicted in waveforms 4a and 4b (the reverse-pulse data were omitted since they provide identical curves). The forward-pulse transition and the reverse-pulse transition in 4a (and in 4b) are identical (symmetric pulses); hence the resulting decay curves are equivalent. Comparing the pulse transitions between waveforms 4a and 4b shows the step for 4b to be smaller in magnitude; hence, the decay curve reflects this difference. Note that in Figure 5, the current difference between these two decay curves becomes greater as the measurement time becomes shorter. At longer measurement times, there is essentially no difference in the background current between waveform 4a and 4b under the conditions in which Figure 5 was obtained. The capacitance value used in these calculations is typical for a carbon electrode. For a platinum electrode (capacitance = 20 μF), the decay curves shown in Figure 6 indicate that only at very short data acquisition times would there be a noticeable difference in the background current.

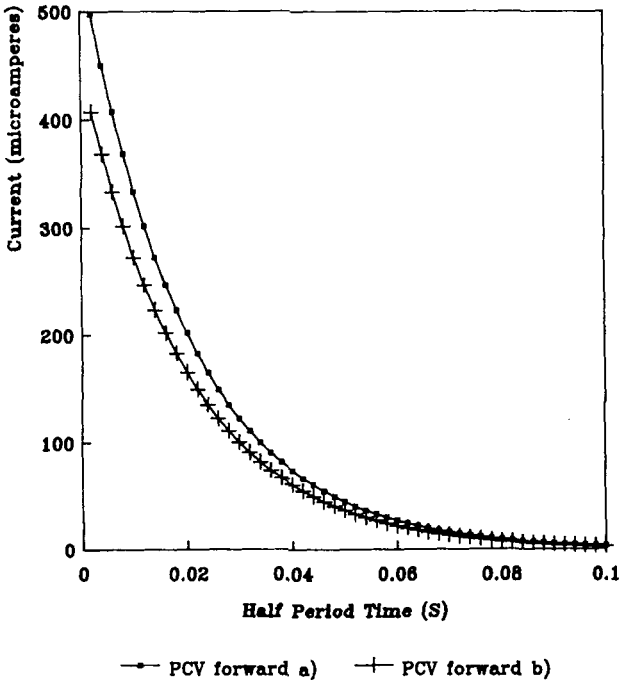

FIGURE 5. Charging current decay curve for a carbon electrode with a PCV excitation waveform.

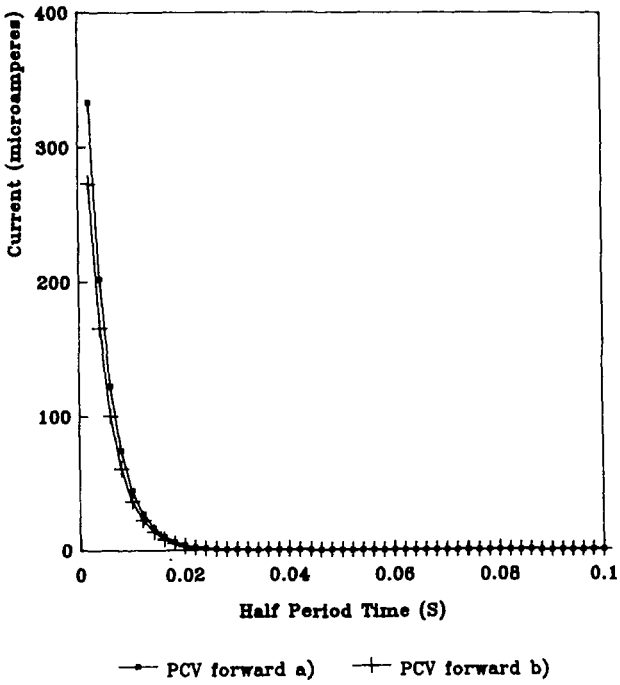

FIGURE 6. Charging current decay curve for a platinum electrode with a PCV excitation waveform.

These results indicate that, for a carbon electrode, with its larger capacitance value, the waveform depicted in Figure 4b offers lower background currents at higher data acquisition frequencies.

The SWCV waveforms shown in Figures 4c and d may be treated in a similar manner; however, the waveform pulse transitions are asym-

metric in each of the two cases. Consider only the waveform in Figure 4d: the forward-pulse transition is larger than the reverse-pulse transition, implying that the matching decay curves are dissimilar. This is illustrated in Figure 7, where the forward current for d (corresponding to waveform 4d) is larger than the reverse current for d. Figure 7 was developed from the same parameters used for Figure 5, except that the forward-pulse transition step was calculated to be 0.120 V and the reverse-pulse transition was 0.100 V. The data in this plot again show that, at higher data acquisition frequencies (shorter half-periods), there is a significant difference in the background current. The current-decay curves for the waveform in Figure 4c are also plotted in Figure 7 (for pulse-transition values of 0.100 V for the forward pulse and 0.080 V for the reverse pulse). It can again be concluded that the forward-pulse current-decay curve provides higher background currents at faster data acquisition times relative to the reverse-pulse current-decay curve.

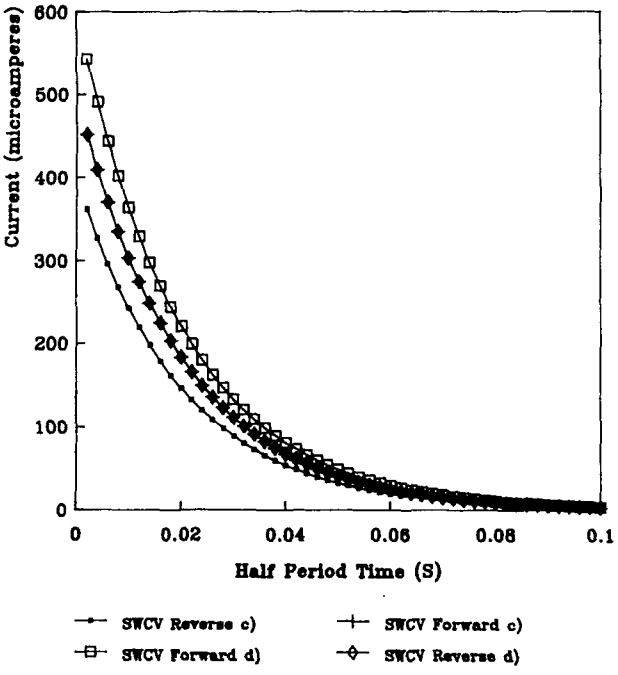

FIGURE 7. Charging current decay curve for a carbon electrode with a SWCV excitation waveform.

As shown for the two PCV waveforms, at longer data acquisition times, there is no significant difference in background currents between the two SWCV waveforms depicted in figures 4c and d. At higher data acquisition rates, the increase in background current is greater for the waveform in Figure 4d than in 4c. The lower-capacitance platinum electrode would also yield decay curves in which the background current differences are negligible (Figure 6), except at extremely short data acquisition times (Figure 8).

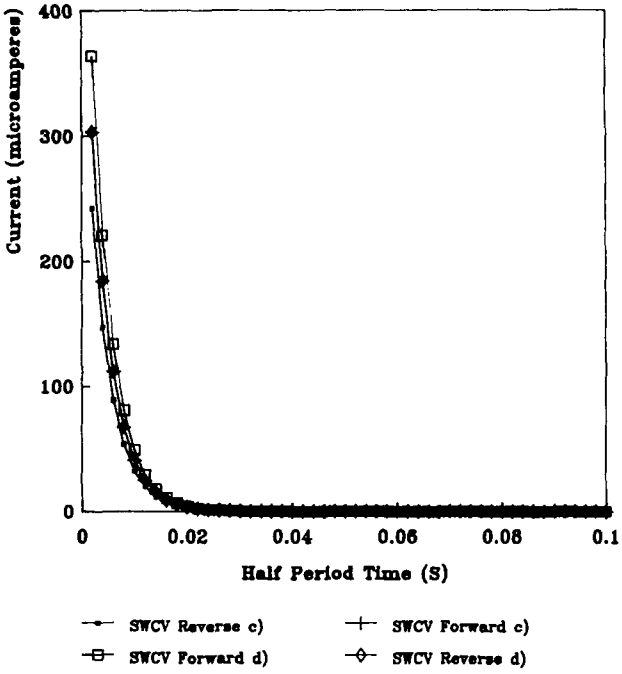

FIGURE 8. Charging current decay curve for a platinum electrode with a SWCV excitation waveform.

The preceding discussion indicates that electrodes with higher capacitance values have background currents that vary significantly for various waveforms, particularly at higher data acquisition frequencies. These conclusions are based on charging-current decay curves without considering the Faradaic current contribution to the measured current. The following section empirically describes measurement methods considering both of these components, and the subse-

quent section of this review considers the theory of the Faradaic element.

B. PCV and SWCV Current vs. Voltage Curves — Empirical Approach

1. Total Current vs. Voltage for a Hypothetical Blank Solution

A total current vs. voltage plot is shown in Figure 9 for a hypothetical blank solution. Reductions and oxidations at the electrode surface are represented above and below the zero-current axis, respectively. The voltage axis is dissected by the switching potential, with the forward scan on the left and the reverse scan on the right. The figure lacks indications of electroactivity other than small background currents near the zero-current axis at the culmination of each decay curve. It is at this point in each decay that it is favorable to measure the current since the charging current has diminished to insignificant proportions, isolating any Faradaic current that may be present.

2. Measured Current vs. Voltage for a Hypothetical Blank Solution

A typical plot of the measured current vs. voltage for a well-behaved blank solution is illustrated in Figure 10. In CV, PCV, and SWCV, the forward scan may be toward more positive or negative potentials, depending on the starting material; hence, the potential axis is not labeled in terms of sign. It is appropriate to represent a slight current response (residual charging current) which is dependent on the data acquisition frequency and the capacitance of the electrode. Faradaic currents from impurities may also be present.

3. Total and Measured Current vs. Voltage for a Hypothetical Reversible Couple

A *total* current vs. voltage plot of a solution containing the oxidized form of a reversible couple is depicted in Figure 11, and the *measured* current vs. voltage is shown in Figure 12, each

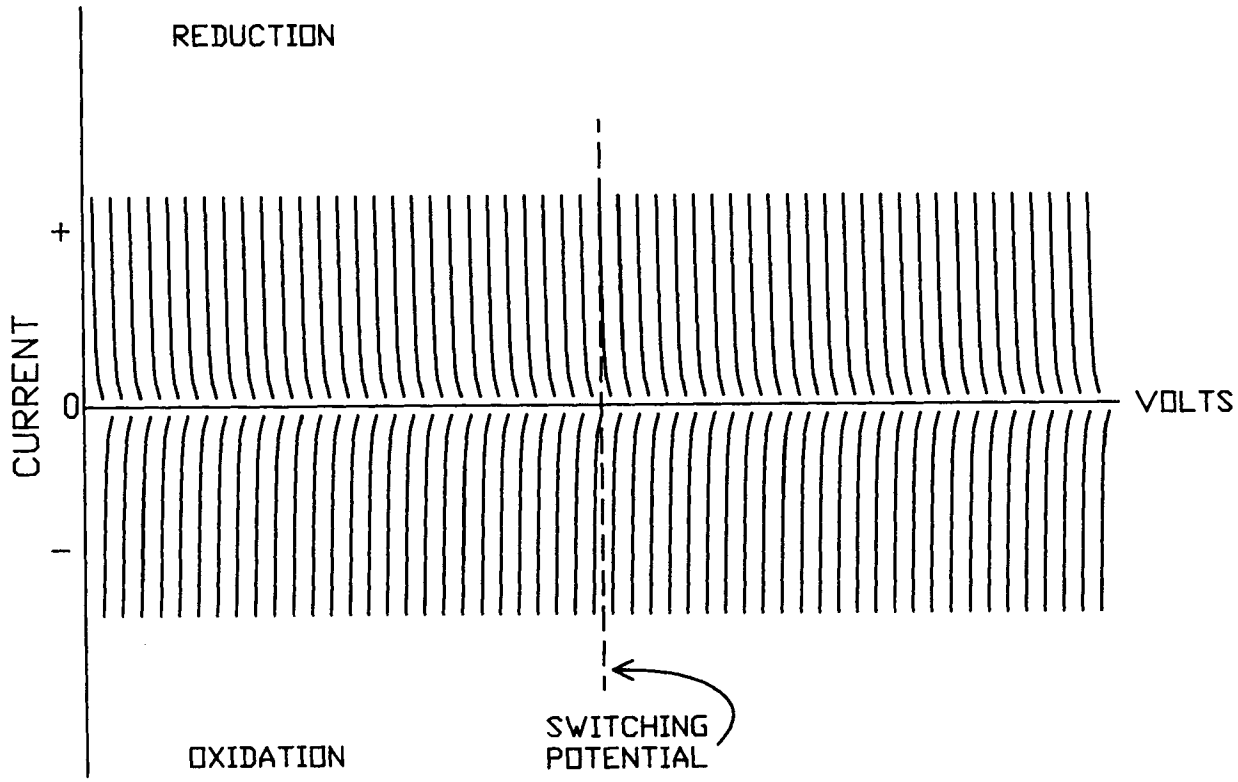

FIGURE 9. Total current vs. voltage (blank solution).

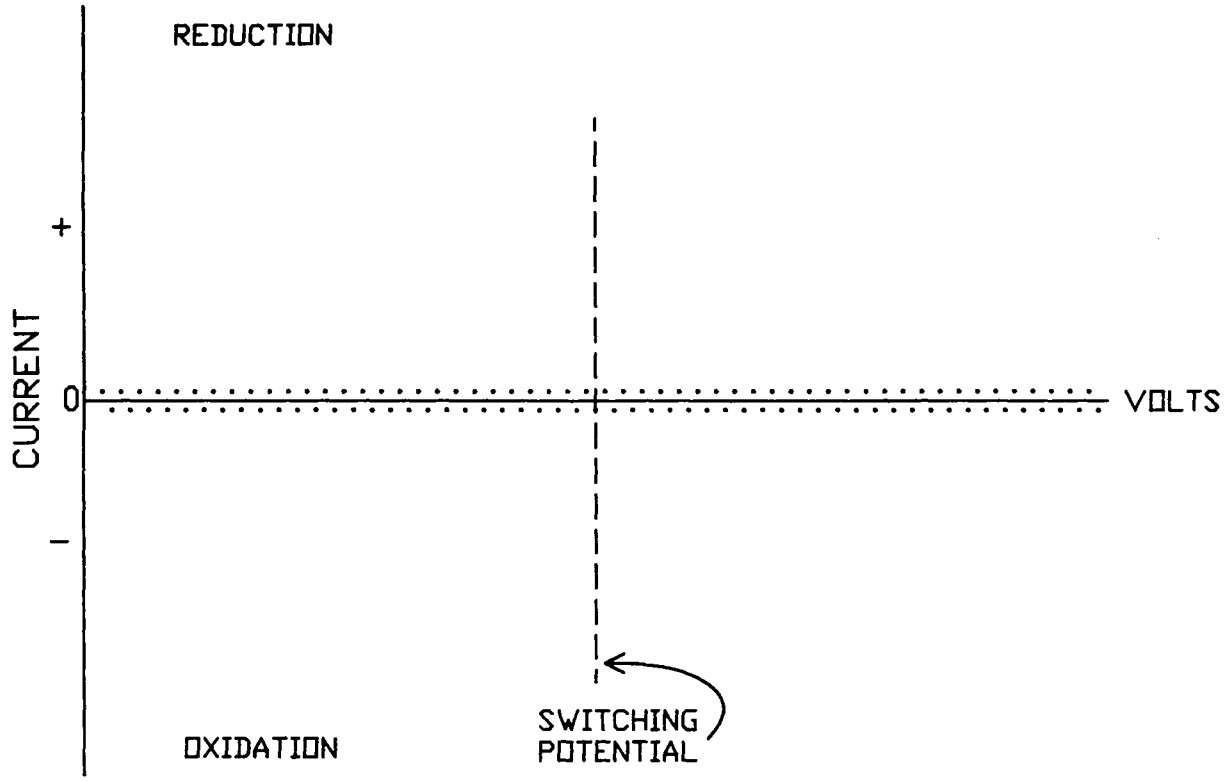

FIGURE 10. Measured current vs. voltage (blank solution).

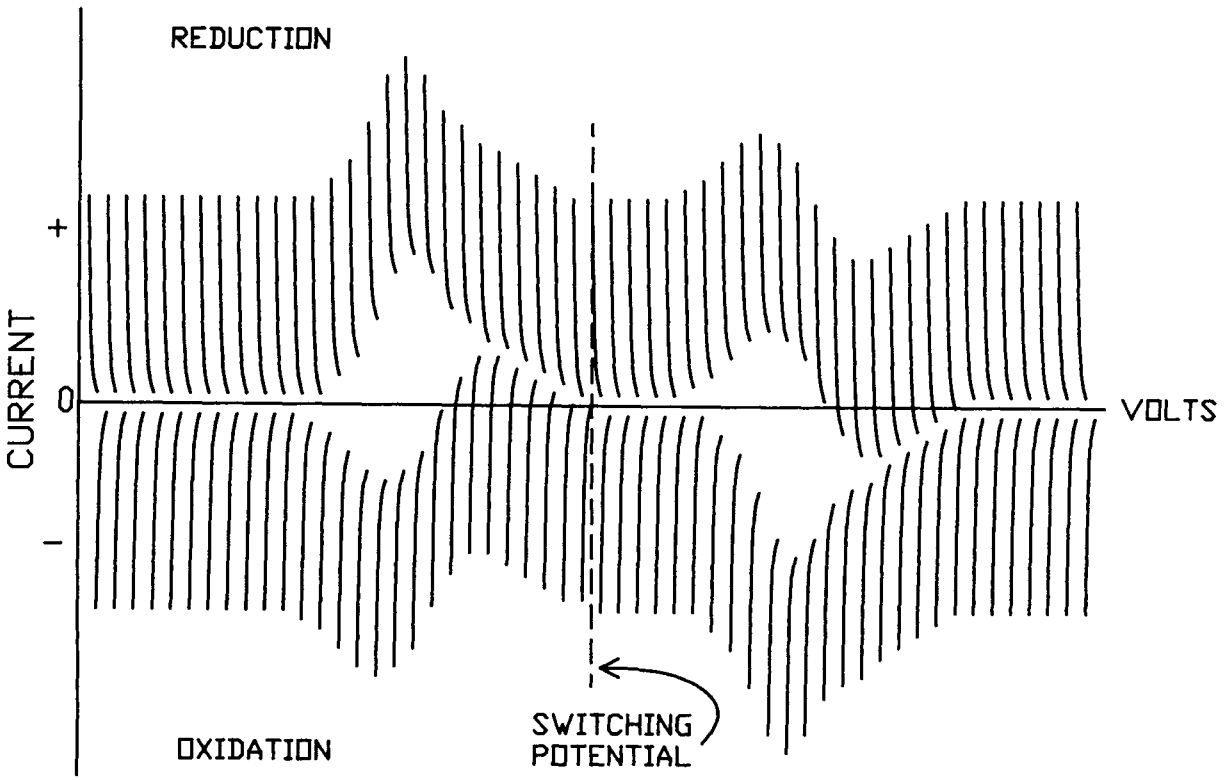

FIGURE 11. Total current vs. voltage (reversible couple).

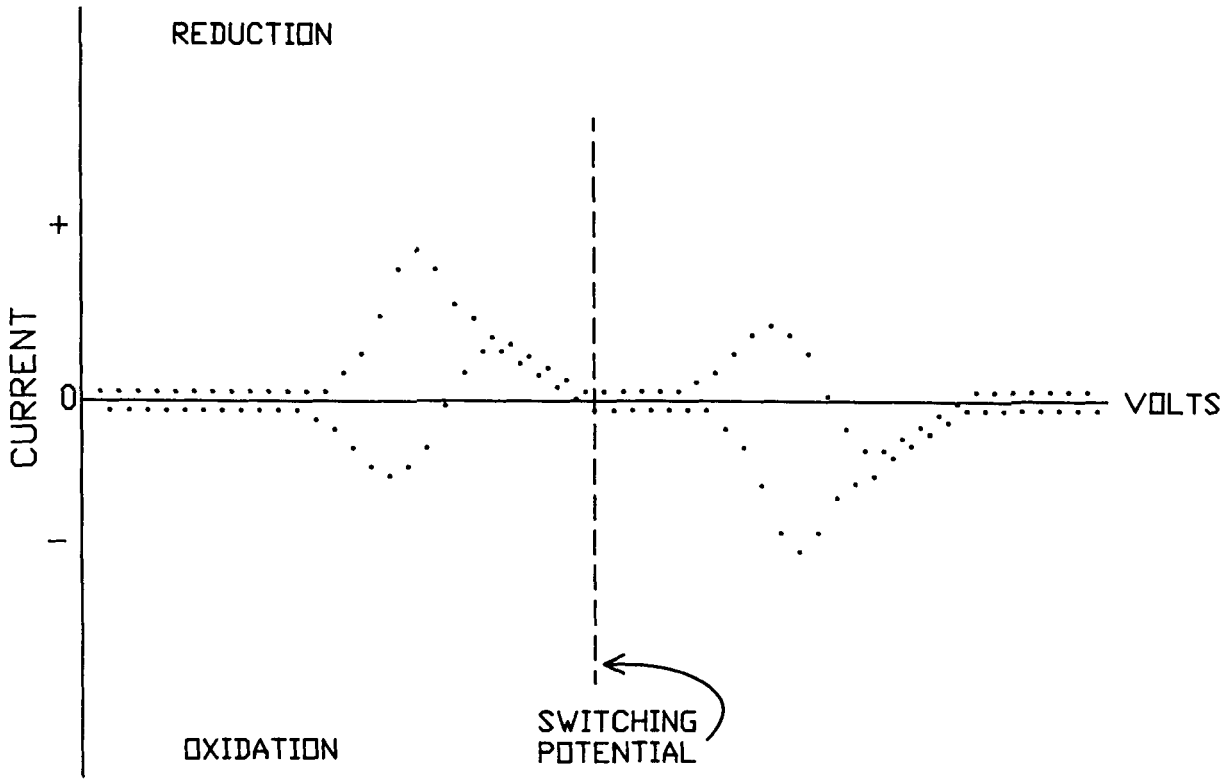

FIGURE 12. Measured current vs. voltage (reversible couple).

showing the occurrence of electrochemical reactions. In the forward scan (left of the switching potential), the major current response is observed on the reduction side of the current axis. The oxidation response is smaller by comparison, due to the short time frame of the pulse. During a forward pulse, when approaching the formal reduction potential of the oxidized species, electrolysis occurs and a reduced species initially absent in the solution is formed at the electrode surface by an amount that depends on the length of the half-period. The reduced species is consequently reoxidized during the reverse pulse, back to the starting material. This process continues until the excitation voltage is sufficiently negative and oxidation ceases to occur.

At still more negative voltages, the diffusion-limited region is entered. At this stage, the area around the electrode surface is void of starting material, and the electrolysis rate relies on the rate of diffusion of the starting material from the bulk solution. At the switching potential, the area surrounding the electrode surface contains only the reduced form of the reversible couple and, by using the same rationale as discussed previously, the minor peak size is smaller, depending on the length of the forward pulse. In the reverse scan, the forward pulses are the downward pulses (see Figure 3) and produce the major oxidation peak. When both scans are complete, the condition at the electrode is returned to the state it was at the start of the scan. In view of this process, this method is considered a nondestructive technique for reversible couples.

4. Difference Current vs. Voltage for a Reversible Couple

For a background current plot (Figure 10), subtracting the first data point below the zero (oxidation side) axis from the first point above this axis (reduction side) gives a net current of zero. Continuing this process provides a straight line superimposed on the zero-current axis, effectively removing the background current from the graph. Applying the same technique to the data in Figure 12 results in background subtrac-

tion and isolation of the Faradaic currents (see Figure 13). The resulting peaks are symmetric, easily identified, and represent the formal reduction potential of the species. This form of data-presentation greatly simplifies the interpretation of results and is amenable to quantitative analysis. Two additional features of this type of plot are that the peaks are positioned in the same direction (absolute-difference current obtained) and contain both reductive and oxidative components. The latter is of importance due to the fact that more current is obtained per molecule of analyte.

5. Measured Current vs. Voltage for a Quasireversible Couple

In addition to the dual time-scale advantage, CV can favorably probe "quasireversible" couples (which are, in a strict sense, irreversible). This term is used by electrochemists because a quasireversible couple can be transformed from one oxidation state to another by applying enough energy to stimulate the conversion, and is accomplished in practice by applying a sufficient activation voltage to the electrode. A representative plot of quasireversible couple is given in Figure 14. Only one major peak is observed as an oxidation in the forward scan. If a square-wave linear-sweep voltammogram were obtained for this arbitrary quasireversible couple, then simply observing the graph would not be sufficient for assessing the degree of reversibility, and further investigation would be necessary. The implied asset of the modified CV plot is that the major peak in the reverse scan in smaller in magnitude and consequently indicates that the couple is quasireversible. These points are elaborated upon later.

This section dealt mainly with the format of current vs. voltage curves for the modified cyclic voltammetry waveforms of Figures 3 and 4, and served to facilitate a clearer understanding of the next sections which consider the theoretical aspects of the Faradaic component of the measured current.

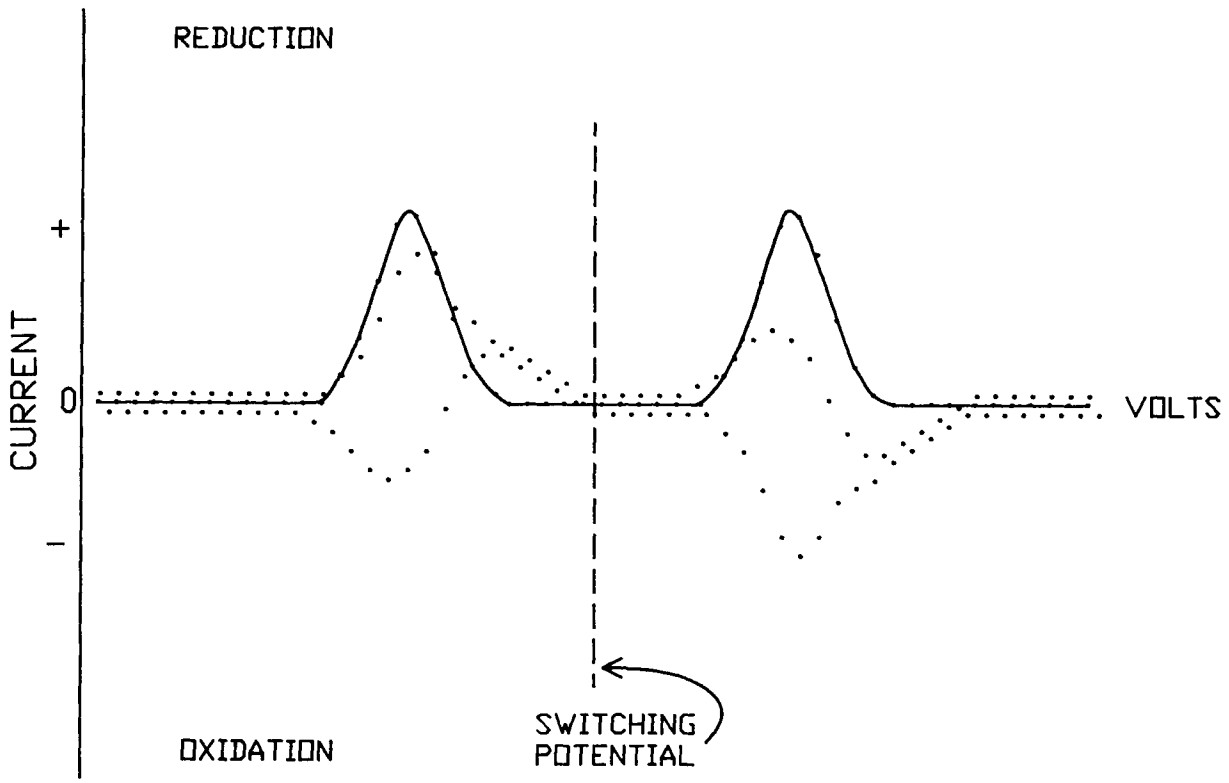

FIGURE 13. Measured current and difference current vs. voltage (reversible couple). Solid line represents the difference current.

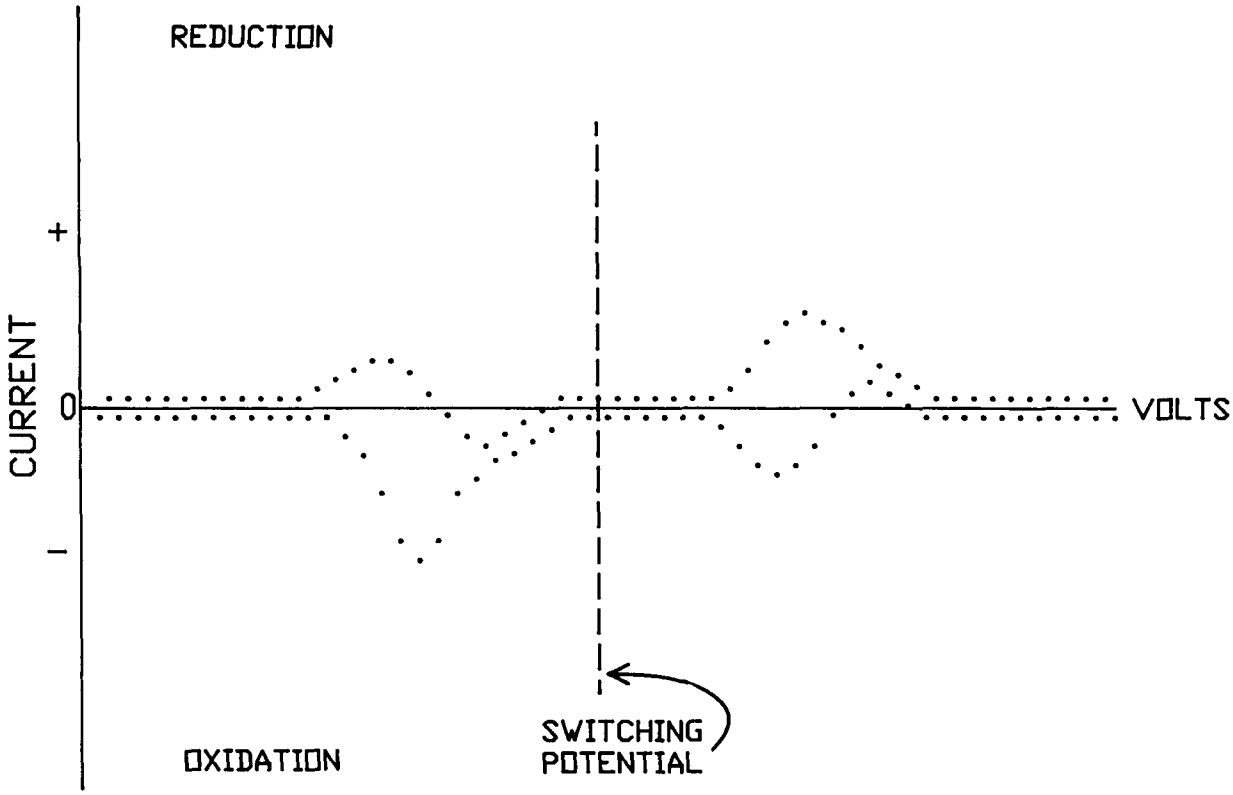

FIGURE 14. Measured current vs. voltage (quasi-reversible couple).

C. Pulse and Square-Wave Cyclic Voltammetry — A Theoretical Treatment

This section considers existing theories related to current-voltage relationships for reversible couples using PCV and SWCV. The following discussions are based on simple reversible electrode reactions of the type

$$O + ne \rightleftharpoons R \tag{5}$$

where 0 represents the only reactant initially present in solution, and R, formed by electrolysis at the electrode surface, dissolves in the solution or the mercury phase. Definitions of the terms employed are given in Table 1.

The initial and boundary conditions in all cases are as follows. For the forward scan

at $t = 0$, $C_{ox} = C^*$, $C_{Red} = 0$, $0 \leqslant x \leqslant \infty$
for $t > 0$, $C_{ox} \rightarrow C^*$, $C_{Red} \rightarrow 0$, $x \rightarrow \infty$

For the reverse scan

at $t = 0$, $C_{Red} = C^*$, $C_{ox} = 0$, $0 \leqslant x \leqslant \infty$
for $t > 0$, $C_{Red} \rightarrow C^*$, $C_{ox} \rightarrow 0$, $x \rightarrow \infty$

1. Pulse Cyclic Voltammetry Theory

Treatment of the forward scan of PCV waveform 1 in Figures 3 and 4 is based on the work of Barker and Jenkins[19] and Krause and Ramaley.[43] The other PCV waveform (waveform b in Figures 3 and 4) is also considered and compared.

For the forward scan and reverse scan

$$i_{diff} = \frac{n^2F^2AD^{1/2}C^*\Delta E}{RT\pi^{1/2}(\sigma\tau)^{1/2}} \times \left[\frac{P}{(1 + P)^2}\right] \times \sum_{m=0}^{\infty}\frac{(-1)^m}{(m + \beta)^{1/2}} \tag{7}$$

TABLE 1
Definitions of Terms

i	= The response current measured (amperes)
i_{dif}	= The difference current response (amperes)
n	= The number of electrons transferred at the electrode surface
F	= Faraday constant (96484.56 C mol^{-1})
R	= Universal gas constant (8.314 JK^{-1} mol^{-1})
T	= Temperature in degrees Kelvin
τ	= Period of the pulse train or square wave (s)
σ	= Fraction of τ for the half-period (0.5 in all cases discussed here)
D_o	= Diffusion coefficient of the oxidized species (cm^2/s)
D_R	= Diffusion coefficient of the reduced species (cm^2/s)
D*	= Can be either D_o or D_R depending on the bulk species in solution
C*	= Either conc. of oxidized or reduced reactant of the bulk solution (mol/cm^3)
C_{ox}	= Concentration of oxidized reactant at the electrode surface
C_{RED}	= Concentration of reduced reactant at the electrode surface
p_1, p_2	= Fractions less than unity where $p_1 < \sigma < p_2$
A	= Area of the electrode (cm^2)
x	= Distance from the electrode in centimeters
t	= Time (s)
E	= The mean potential at which the current is measured (V)
E_i	= The initial starting potential
E_s	= The switching potential
E^o	= The standard reduction potential (V)

$$E_{1/2} = E^o + \frac{RT}{2nF} \ln \frac{D_R}{D_o} \qquad (6)$$

where $P = \exp(E - E_{1/2})\, nF/RT$ for the forward scan, $P = \exp -(E - E_{1/2})\, nF/RT$ for the reverse scan, ΔE is the peak-to-peak voltage of the square wave, C* is the concentration of the oxidized or reduced reactant, D* is the diffusion coefficient of the oxidized or reduced reactant, and $\beta = p_2\sigma\tau$ (see other terms in Table 1).

Equation 7 was used to prepare the difference current vs. voltage curves of Figure 15 for both PCV waveforms. The following parameter values were used in the calculations:

A	1 cm^2
D*	4.5×10^{-6} cm^2/s
C*	1×10^{-6} mol/cm^3 (0.001 *M*)
T	298 K
n	1 electron
τ	0.020 s
p_2	0.999
$E_{1/2}$	0.300 V
ΔE	0.110 V for PCV type a
ΔE	0.090 V for PCV type b

The theory presented by Barker[19] was restricted to $\Delta E < 0.5$ RTnF, where ΔE represents the peak-to-peak square-wave amplitude. Implementing higher ΔE values (as is the case here) affects the half-width of the peak and other parameters. Figure 15 clearly shows that PCV waveform a offers (see Figure 3) a superior sensitivity in terms of the Faradaic current component at the concentration used in the calculation. At lower concentrations, it may be advantageous to use waveform b, due to the reduced background current obtained with this signal at a carbon electrode (e.g., the background current measured at $\tau = 0.020$ s; [see Figure 5 at 0.010 s] for waveform a is 333 μA, and for waveform b it is 273 μA, a difference of 60 μA).

2. Square-Wave Cyclic Voltammetry Theory — Type I

The relationships for the forward scan of waveform type c (Figures 3c and 4c), worked out by Krause and Ramaley,[43] are given as:

For the forward scan

$$i_{FOR} = \frac{nFAD_o^{1/2}C^*}{\pi^{1/2}(\sigma\tau)^{1/2}} \left[\frac{1 - Q_1}{(j - 1 + p_2)^{1/2}} + \frac{Q_1 - Q_2}{(j - 2 + p_2)^{1/2}} + \cdots + \frac{Q_{j-1} - Q_j}{(p_2)^{1/2}} \right] \qquad (8)$$

where i_{FOR} = forward scan currents and

$$C^*Q_j = C^* \left[\frac{\exp(E_j - E_{1/2})nF/RT}{1 + \exp(E_j - E_{1/2})nF/RT} \right] \qquad (9)$$

$$E_j = E_i - j\Delta E - (-1)^j E_{sw} \qquad (10)$$

where $1 < j < \infty$.

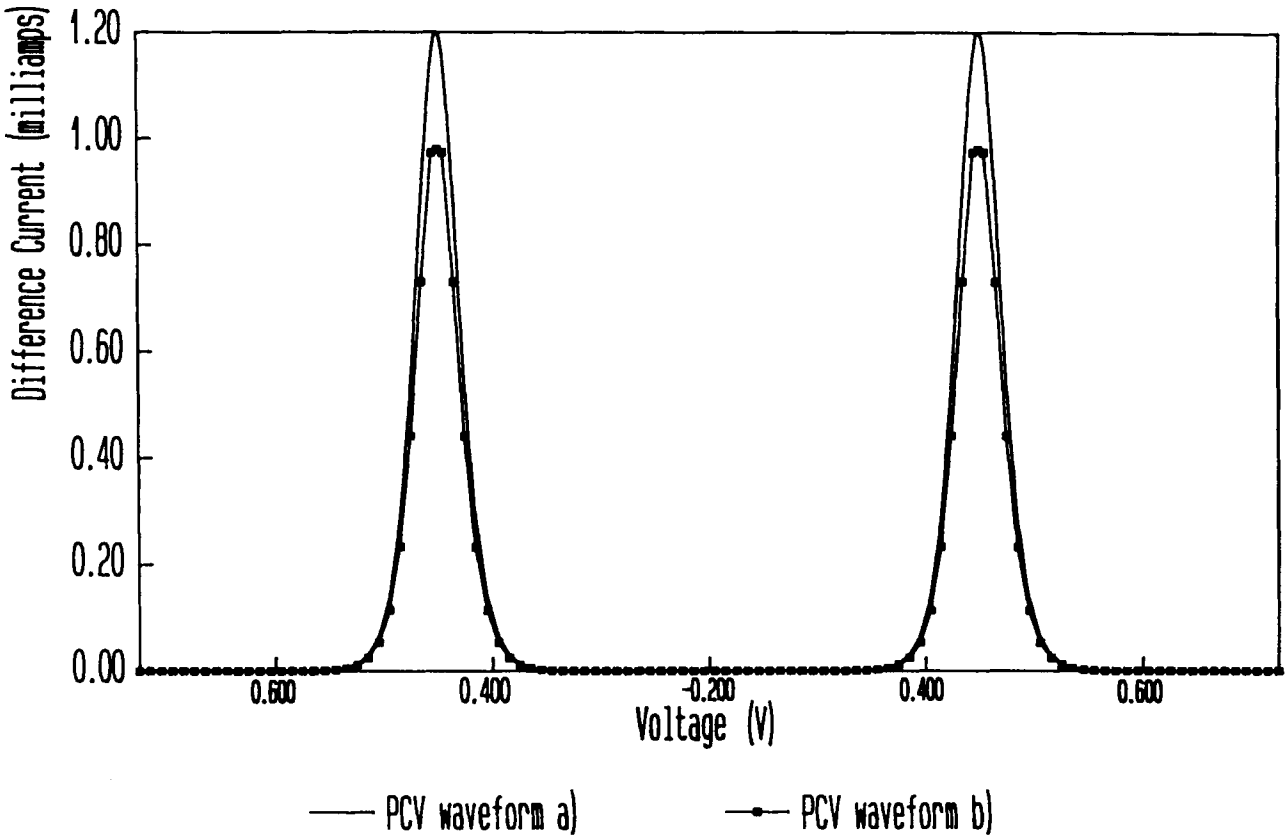

FIGURE 15. Comparison of theoretical difference current vs. voltage plots for two PCV waveforms.

For the reverse scan

$$i_{REV} = \frac{-nFAD_R^{1/2}C^*}{\pi^{1/2}(\sigma\tau)^{1/2}}\left[\frac{1 - Q_1}{(j - 1 + p_2)^{1/2}} + \frac{Q_1 - Q_2}{(j - 2 + p_2)^{1/2}} + \cdots + \frac{Q_{j-1} - Q_j}{(p_2)^{1/2}}\right] \quad (11)$$

where i_{REV} = reverse scan currents and

$$C^*Q_j = C^*\left[\frac{\exp - (E_j - E_{1/2})nF/RT}{1 + \exp - (E_j - E_{1/2})nF/RT}\right] \quad (12)$$

$$E^j = E_i + j\Delta E + (-1)_j E_{sw} \quad (13)$$

where $1 < j < \infty$.

The following parameter values were used in the calculations for the results shown in Figure 16:

A	1 cm²
D_*	4.5×10^{-6} cm²/s
C_*	1×10^{-6} mol/cm³ (0.001 *M*)
T	298 K
n	1 electron
τ	0.020 s
p_2	0.999
E_i	0.0800
E_s	−0.200
$E_{1/2}$	0.300 V
E_{sw}	0.100 V

In contrast to the PCV plots described earlier, in SWCV the forward and reverse currents are displayed during the forward and reverse scans. A difference current may be obtained by plotting the absolute difference between the two points taken during a voltage period (discussed in more detail later). The forward and reverse plots provide additional information about the electrochemical processes that occur at the electrode surface. For example, Figure 16 shows two reductions and two oxidations (the difference plot

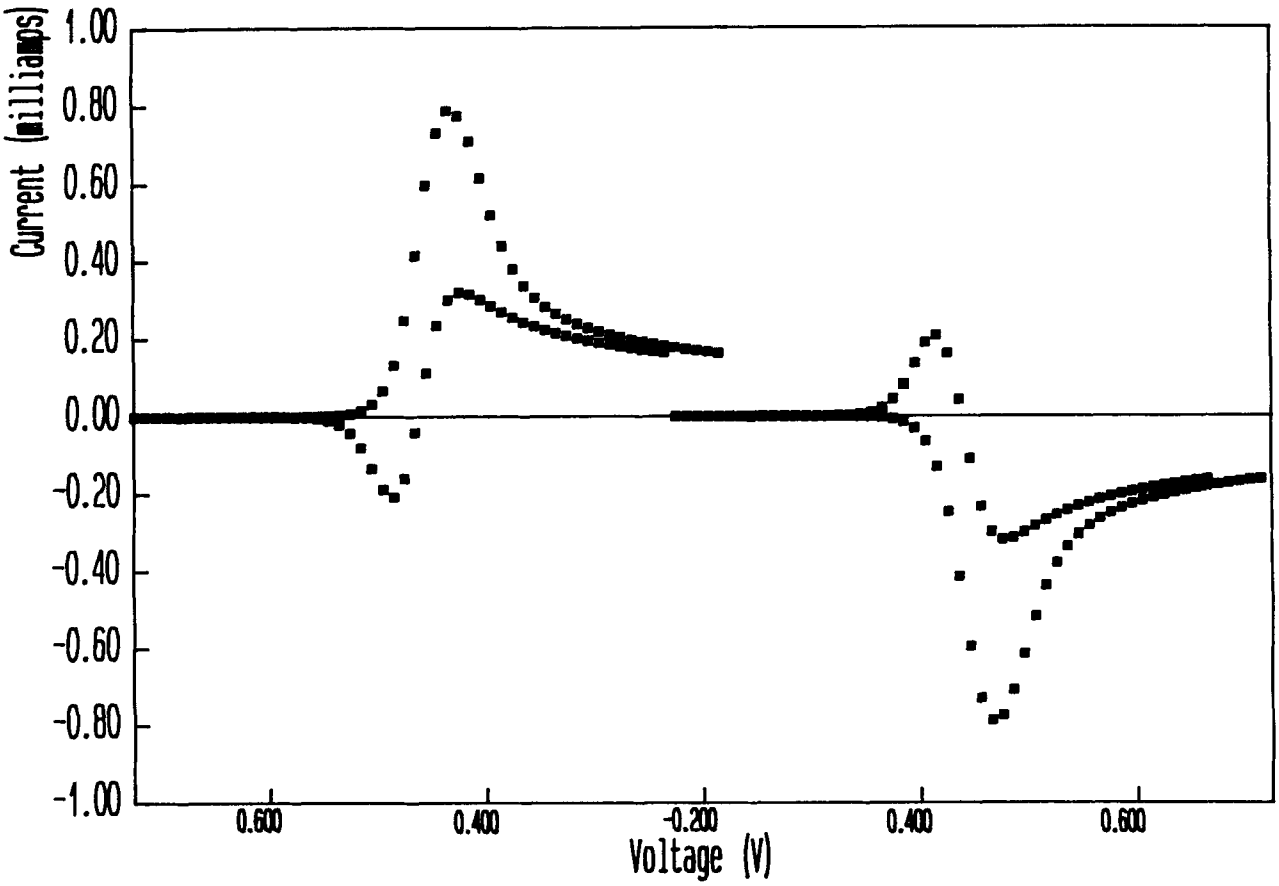

FIGURE 16. Theoretical forward and reverse currents vs. voltage plot for the SWCV Type I waveforms.

of these data contains only two peaks, each representing the sum of the short time-scale reduction and oxidation currents); for qualitative work, then, the forward and reverse currents are more informative.

3. Square-Wave Cyclic Voltammetry Theory — Type II

The relationships for the forward scan of waveform type d (Figures 3d and 4d), investigated by Christie et al.,[39] are given as:

For the forward scan: for a planar electrode, the surface concentration of the oxidized reactant is fixed by:

$$C_{ox}(0,t) = \frac{C^*}{1 + \epsilon} \quad (14)$$

$$\epsilon(t) = \exp\left[- \frac{nF}{RT} [E(t) - E_{1/2}] \right] \quad (15)$$

and the potential waveforms are

$$E_1(k) = E_i - k\Delta E - E_{sw} \quad (16)$$

$$E_2(k) = E_i - k\Delta E + E_{sw} \quad (17)$$

where $k < 1 < \infty$.

For the forward scan: the forward current during the jth period, measured at $p_2\tau$, and the reverse current during the same period, measured

at $p_2\tau$, are described, respectively, by the following two expressions:

$$i_{FOR} = \frac{nFAD_o^{1/2}}{\pi^{1/2}\tau^{1/2}}\left[\frac{C^2(j-1) - C_1(j)}{(p_1)^{1/2}} + \sum_{m=0}^{j-1}\left[\frac{C_2(m-1) - C_1(m)}{(j-m+p_1)^{1/2}} + \frac{C_1(m) - C_2(m)}{(j-m+p_1)^{1/2}} + \frac{C_1(m) - C_2(m)}{(j-m+p_1-\sigma)^{1/2}}\right]\right] \quad (18)$$

where i_{FOR} = forward pulse currents, and

$$i_{REV} = \frac{nFAD_o^{1/2}}{\pi^{1/2}\tau^{1/2}}\sum_{m=0}^{j}\left[\frac{C_2(m-1) - C_1(m)}{(j-m+p_2)^{1/2}} + \frac{C_1(m) - C_2(m)}{(j-m+p_2-\sigma)^{1/2}}\right] \quad (19)$$

where i_{REV} = reverse pulse currents.

In Equations 18 and 19, terms of the type $C_1(k)$ represent the surface concentrations of the oxidized species during the forward pulse of the *k*th period; terms of the form $C_2(k-1)$ and $C_2(k)$ represent the surface concentrations during the reverse pulses of the $(k-1)$ and *k*th periods, respectively. (n.b., numbering of the period starts with $j = 0$, and $C_2(-1)$ [for the first period] is the bulk concentration C*.)

For the reverse scan: for a planar electrode, the surface concentation of the reduced species is fixed by:

$$C_{RED}(0,t) = \frac{C^*}{1+\epsilon} \quad (20)$$

where

$$\epsilon(t) = \exp\left[\frac{nF}{RT}[E(t) - E_{1/2}]\right] \quad (21)$$

and the potential waveforms are

$$E_1(k) = E_i + k\Delta E + E_{sw} \quad (22)$$

$$E_2(k) = E_i + k\Delta E - E_{sw} \quad (23)$$

where $k < 1 < \infty$.

For the reverse scan: the forward current during the jth period, measured at $p_1\tau$, and the reverse current during the same period, measured at $p_2\tau$, are described, respectively, by the following two expressions:

$$i_{FOR} = \frac{-nFAD_o^{1/2}}{\pi^{1/2}\tau^{1/2}}\left[\frac{C_2(j-1) - C_1(j)}{(p_1)^{1/2}} + \sum_{m=0}^{j-1}\left[\frac{C_2(m-1) - C_1(m)}{(j-m+p_1)^{1/2}} + \frac{C_1(m) - C_2(m)}{(j-m+p_2-\sigma)^{1/2}}\right]\right] \quad (24)$$

where i_{FOR} = forward pulse currents, and

$$i_{REV} = \frac{-nFAD_o^{1/2}}{\pi^{1/2}\tau^{1/2}} \times \sum_{m=0}^{j}\left[\frac{C_2(m-1) - C_1(m)}{(j-m+p_2)^{1/2}} + \frac{C_1(m) - C_2(m)}{(j-m+p_2-\sigma)^{1/2}}\right] \quad (25)$$

where i_{REV} = reverse pulse currents.

The C terms are as described above for the forward scan.

The forward- and reverse-pulse currents for the forward and reverse scans (Equations 18, 19, 24, and 25) are plotted against the voltage values (Equations 16, 17, 22, and 23) in Figure 17, using the following parameter values:

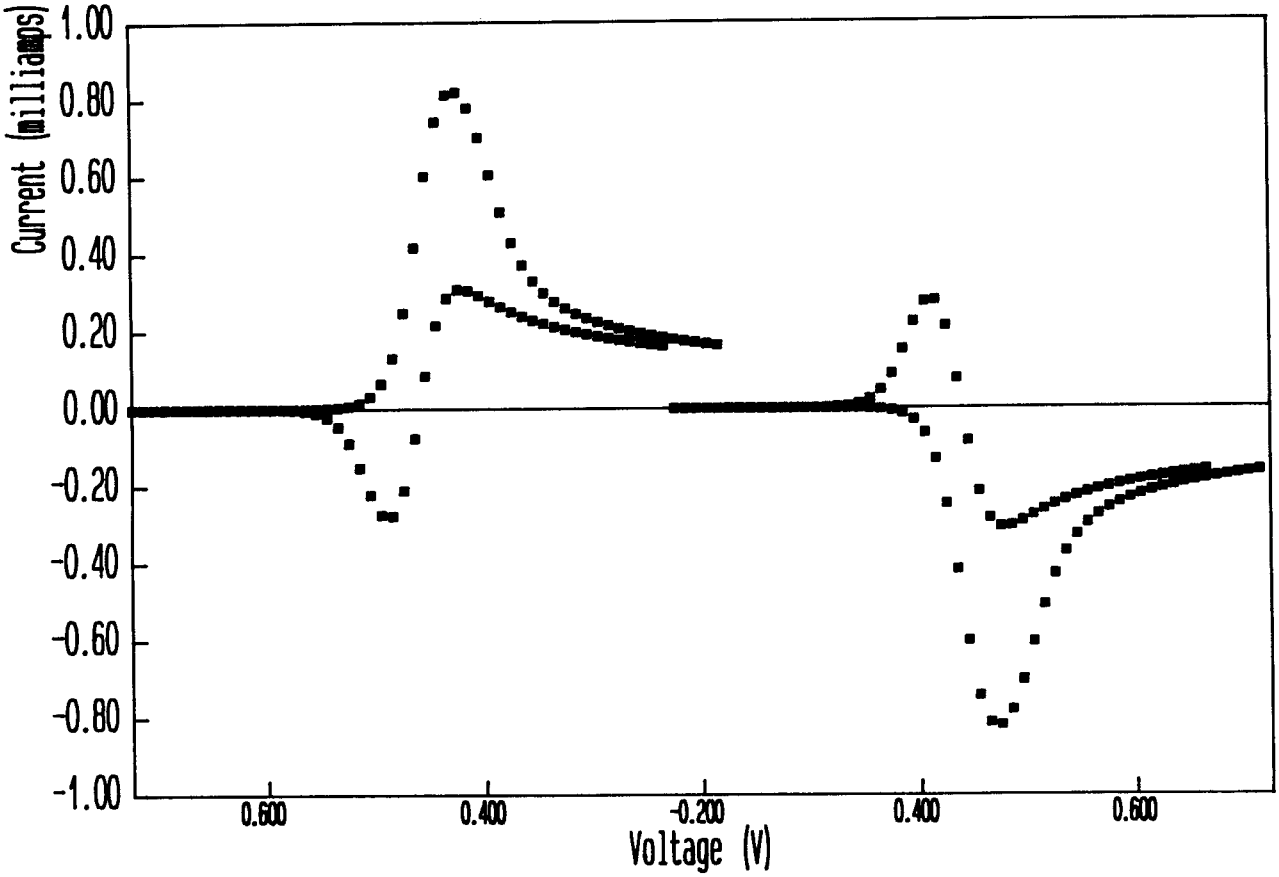

FIGURE 17. Theoretical forward and reverse currents vs. voltage for the SWCV Type II waveforms.

A	1 cm^2
D_*	4.5×10^{-6} cm^2/s
C_*	1×10^{-6} mol/cm^3 (0.001 *M*)
T	298 K
n	1 electron
τ	0.020 s
p_1	0.499
p_2	0.999
E_1	0.800
E_s	−0.200
$E_{1/2}$	0.300 V
E_{sw}	0.100 V

4. Difference Current vs. Voltage Comparison of SWCV Type I and II Waveforms

Figure 18 shows the difference current vs. voltage plot for SWCV waveforms of Types I and II (waveform types c and d, respectively). The difference currents were obtained by taking the absolute difference between period pulse currents of the data shown in Figures 16 and 17. Figure 18 indicates that SWCV waveform Type II offers slightly better sensitivity in terms of total current. Using a carbon electrode (see Figure 7), SWCV waveform type I offers lower background currents. Since for each pulse period (see Figure 4) the pulse amplitudes are symmetric, at higher data acquisition frequencies, the process of subtracting the pulse currents results in nonzero-difference currents. For example, see the SWCV forward d pulse current and the SWCV reverse d pulse current at a half-period time of 0.02 s in Figure 7: clearly, subtraction of these two currents yields a bias current in favor of the larger forward-pulse current; hence, the electrode capacitance plays a significant role in the determination of these currents.

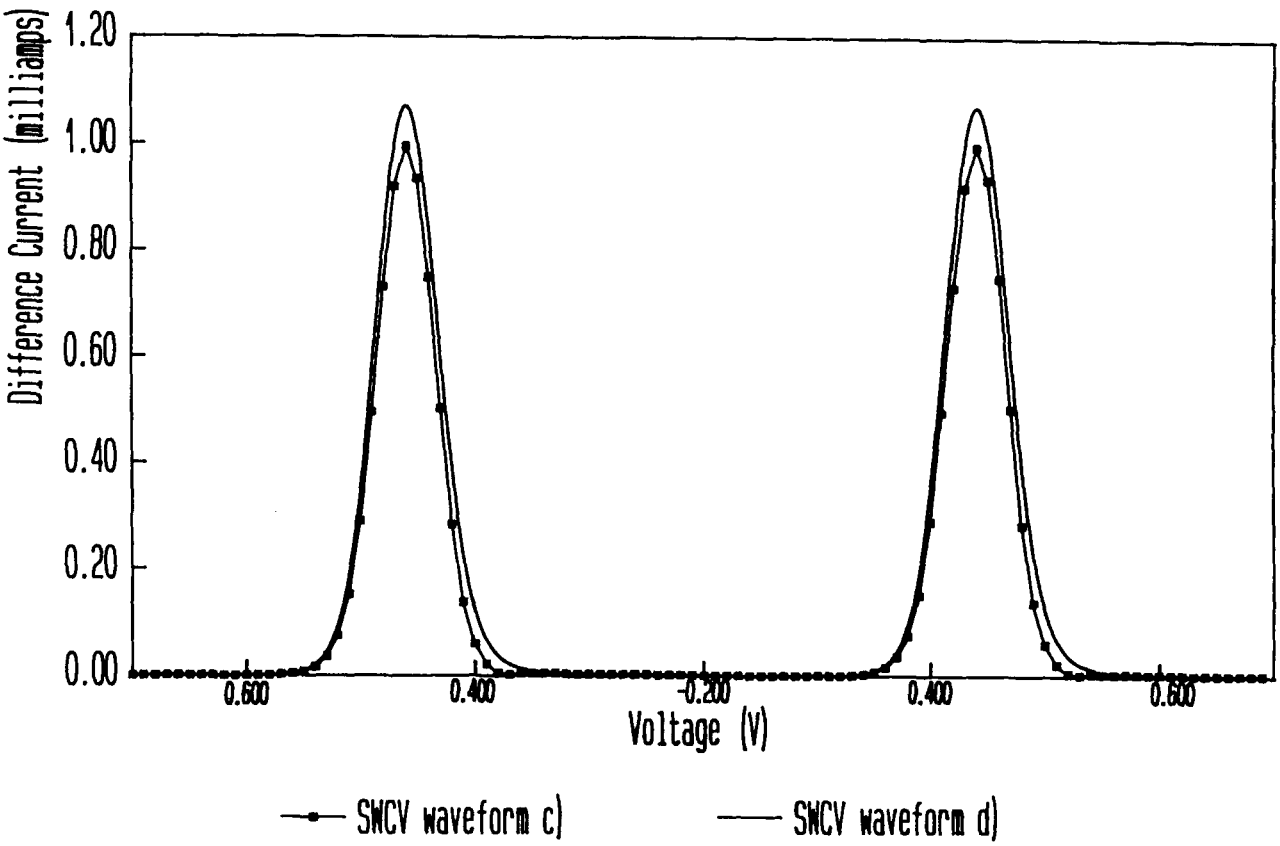

FIGURE 18. Comparison of theoretical difference current vs. voltage plots for two SWCV waveforms.

IV. APPLICATIONS OF PULSE AND SQUARE-WAVE CYCLIC VOLTAMMETRY TO STATIC SOLUTIONS

A. General Overview

Drake et al.[45] demonstrated that cyclic differential-pulse voltammetry provides qualitative estimations of differential pulse behavior. In their studies, they used variable DC scan rates to evaluate the nature of the measurement in terms of both the DC and pulse components of the experiment. Using this technique for multicomponent analysis, Eccles and Purdy[50] showed that well-defined, easily resolved peaks result, as opposed to the semi-peak readout for CV. These latter workers demonstrated that, by combining CV with a pulse technique, quantitative determinations were possible (using the ferricyanide-ferrocyanide couple as the example). The theoretical model for reversible couples at the dropping mercury electrode was presented by Ramaley and Tan.[48] However, comparing theory and experiment for systems in which the product is soluble in both solution and the electrode, indicated that, for reversible electrochemical reactions, the theory is strictly applicable only to the solution-soluble case.

B. Effect of the Transfer Coefficient on Voltammogram Symmetry

The work of Drake et al.[45] further showed that quasireversible charge transfer will lead to increased separation of the peaks for the forward and reverse scan directions and to peak heights of unequal magnitude. The PCV work of Eccles and Purdy[50] presented evidence of this for the quinone-hydroquinone couple.

The transfer coefficient may be estimated from the following relationship for an irreversible process[54]

$$i_{p(irr)} = 602n(\alpha n_a)^{1/2}AD_o^{1/2}\nu^{1/2}C_o^*(0.4958) \quad (26)$$

where A and D_o are as in Table 1, $i_{p(irr)}$ is the peak current, n is the electron stoichiometry, α is the transfer coefficient, n_a is the number of electrons transferred in the rate-determining step ν is the scan rate, C_o^* is the bulk concentration of the electroactive species, and 0.4958 is a current function maximum for irreversible charge transfer.[55] The transfer coefficient is obtained from the slope of a plot of $i_{p(irr)}$ vs. ν.

Eccles[56] estimated the transfer coefficient to be 0.32 for a solution of hydroquinone in 2 *M* H_2SO_4. Nicholson[57] studied the effect of the charge transfer coefficient on the symmetry of cyclic voltammograms and found that for $\alpha < 0.5$, the cathodic peak is more rounded than the anodic peak. This broadening also results in a lowering of peak height. For $\alpha > 0.5$, the converse holds.

Figure 19 (redrawn data from Figure 6 of Reference 50) shows a PCV voltammogram for 1 m*M* quinone in 1 *M* sulfuric acid. The two peaks on the left-hand side of the figure (i.e., to the left of the −0.200 V switching potential) illustrates what occurs during the forward scan. The major peak in the positive microampere region (peak potential = 0.266 V vs. Ag/AgCl) represents the reduction current for the conversion of quinone to hydroquinone and is obtained from the upward pulses of the applied waveform (see Figure 3). The minor peak (peak potential = 0.463 V vs. Ag/AgCl) represents the oxidation of hydroquinone during the downward pulses. The latter data are obtained during a short time scale with respect to the upward pulses of the same periods.

On the right-hand side of Figure 19, the major negative peak is the oxidation current (peak potential = 0.477 V vs. Ag/AgCl), obtained from the downward pulses in the reverse scan. These data were taken at a later time (long time scale)

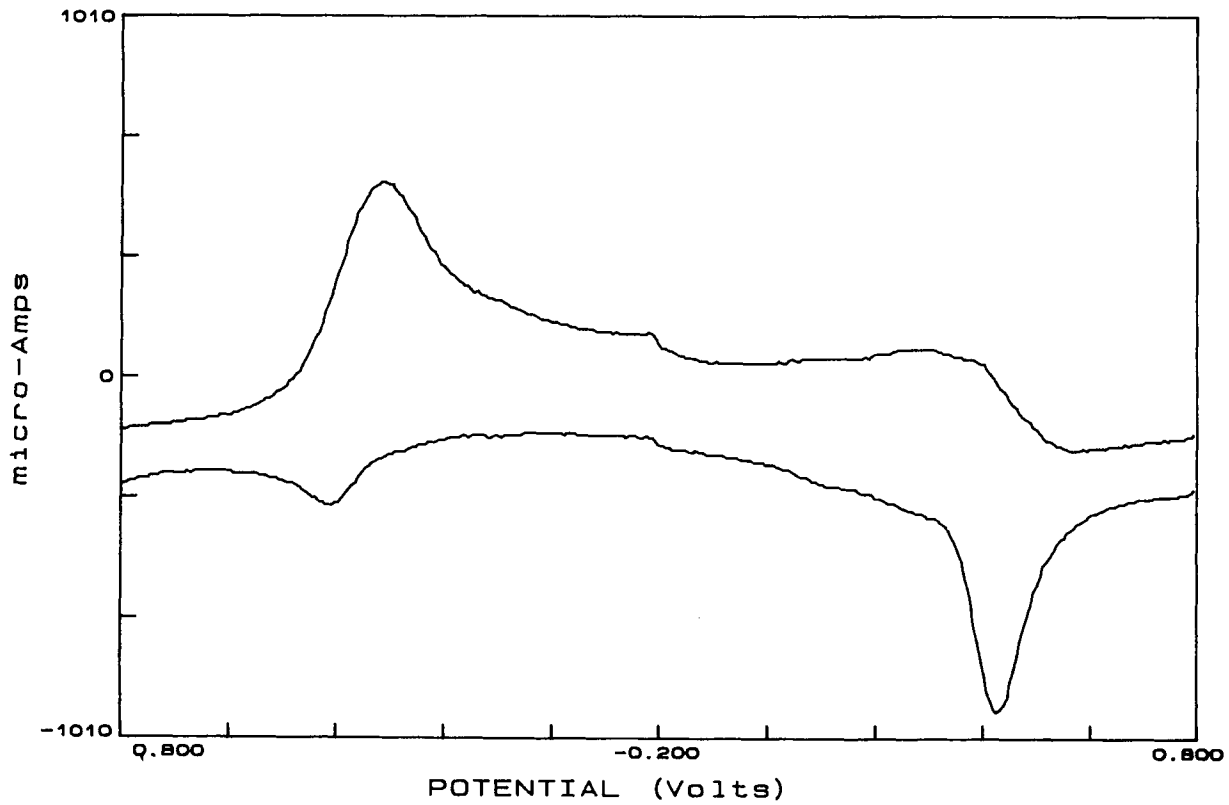

FIGURE 19. Third cycle of a multiple-scan pulse cyclic voltammogram of 1 m*M* quinone in 1 *M* sulfuric acid. Number of cycles, 5; data acquisition frequency, 130 Hz; square-wave frequency, 65 Hz; square-wave amplitude, 100 mV; voltage ramp, 100 mV/s.

relative to the downward pulse data of the forward scan. The poorly defined hump in the upper trace (peak potential = approximately 0.305 V vs. Ag/AgCL) is attributed to the reduction current taken in the short time scale. It is clear from the difference plot of these data (Figure 20) that the height of the reverse-scan peak exceeds that of the forward scan, and that the shapes are different. The peak potentials for the two peaks in Figure 20 (left to right) are 0.324 and 0.412 V vs. Ag/AgCl. The degree of separation in the peak potentials suggests that this couple might be quasireversible. Since α for this couple is 0.32, the cathodic peaks being more rounded than the oxidation peaks is not unexpected (consistent with the work of Nicholson.[57]) Figure 20 shows these symmetry differences and indicates that PCV may also be used in determining the reversibility of a couple in solution. Figure 21 (redrawn from Figure 8 of Reference 50) indicates that the same conclusions can be drawn for a solution of 1 m*M* hydroquinone in 1 M H_2SO_4, based on the transfer coefficient and peak heights for the reversibility of the couple (peak potentials, left to right, are 0.409 and 0.369 V vs. Ag/AgCl). The separation is also an indication of the reversibility.

C. Comparison of PCV and SWCV: *O*-Dianisidine Study

Eccles compared PCV and SWCV (waveforms a and d, respectively, in Figure 3) using solutions of *O*-dianisidine in 1 *M* H_2SO_4[58] and an experimental apparatus which had been described previously.[50] The peak currents obtained for both types of waveforms are plotted against the concentration of *O*-dianisidine in Figure 22. The SWCV and PCV forward-scan data show little relative difference in sensitivity, as do the reverse scans. As expected ramping of the applied voltage during the lifetime of a pulse (waveform a) contributed to the background current (as compared to the use of a constant voltage

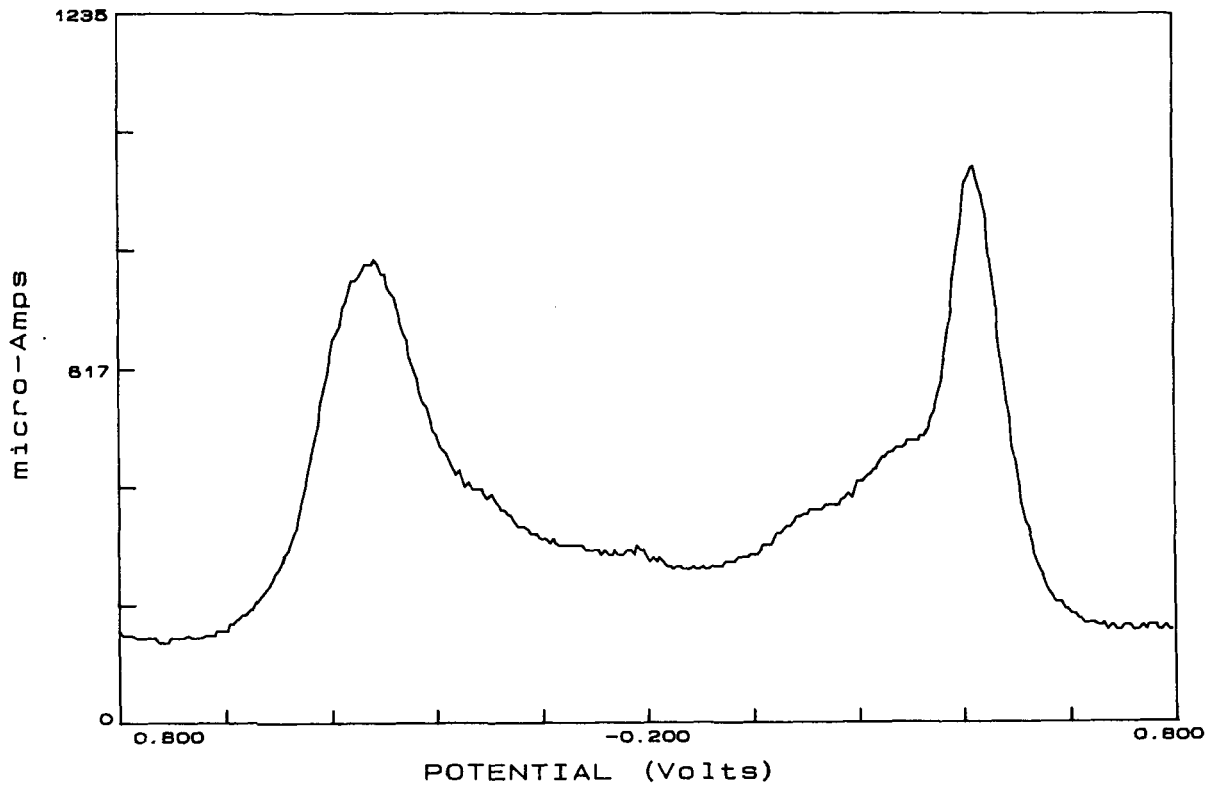

FIGURE 20. Third cycle of a multiple-scan difference pulse cyclic voltammogram of 1 m*M* quinone in 1 *M* sulfuric acid. Number of cycles, 5; data acquisition frequency, 130 Hz; square-wave frequency, 65 Hz; square-wave amplitude, 100 mV; voltage ramp, 100 mV/s.

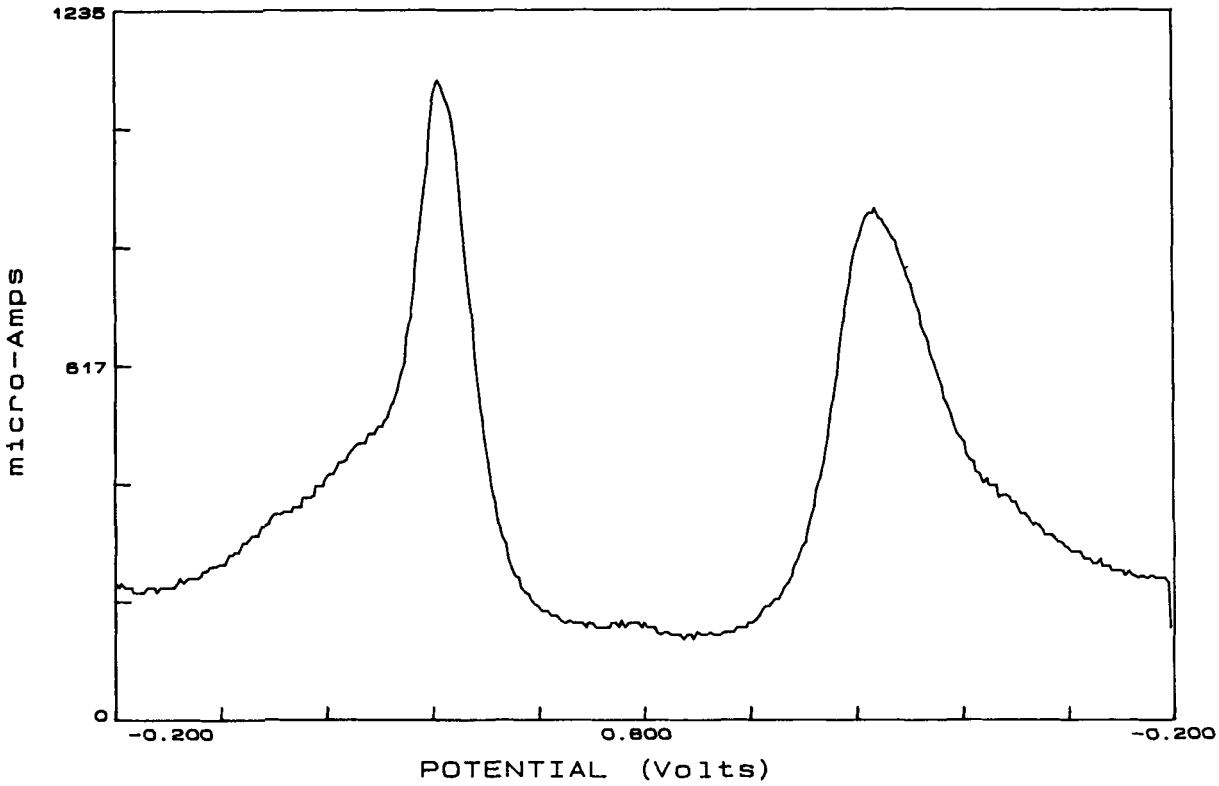

FIGURE 21. Third cycle of a multiple-scan difference pulse cyclic voltammogram of 1 m*M* hydroquinone in 1 *M* sulfuric acid. Number of cycles, 5; data acquisition frequency, 130 Hz; square-wave frequency, 65 Hz; square-wave amplitude, 100 mV; voltage ramp, 100 mV/s.

during the life of a pulse [waveform d]). This has been observed with mercury and platinum electrodes. Carbon electrodes, on the other hand, having higher capacitances, display different characteristics. It might be that the current-decay curve due to pulse transitions is so dominant that, at faster data acquisition times, any contribution from the linearly changing ramp is insignificant. This might explain why the SWCV data in Figure 22 are not significantly higher in sensitivity. Clearly, further studies are needed.

V. APPLICATIONS OF PULSE AND SQUARE-WAVE CYCLIC VOLTAMMETRY TO FLOWING SOLUTIONS

A. Conventional Amperometric Detection

Since Kissinger et al.[59] introduced an inexpensive electrochemical detector for liquid chromatography with picogram sensitivity, a considerable number of instrumental and analytical studies have been carried out and many reviews have appeared.[60-64] Theoretical studies of channel electrodes were conducted by Matsuda[65] using conditions in which the diffusion layer was small with respect to the height of the channel. Later, Weber and Purdy[56] provided an expression relating the current for a rectangular channel-type flow-through electrode to the volume flow rate of the solution, cell dimensions, and physical constants. Such information is useful for optimizing electrochemical cell design for trace analysis, requiring detection at low currents.

Some electrochemical detectors have uitilized carbon paste or glassy carbon as the working surface, and several manufacturers are turning their interest to these carbon-based electrodes.[67] Future markets may include parallel-opposed, dual-working electrode detectors[62] and rapid-scan detectors (described later). The basic technology

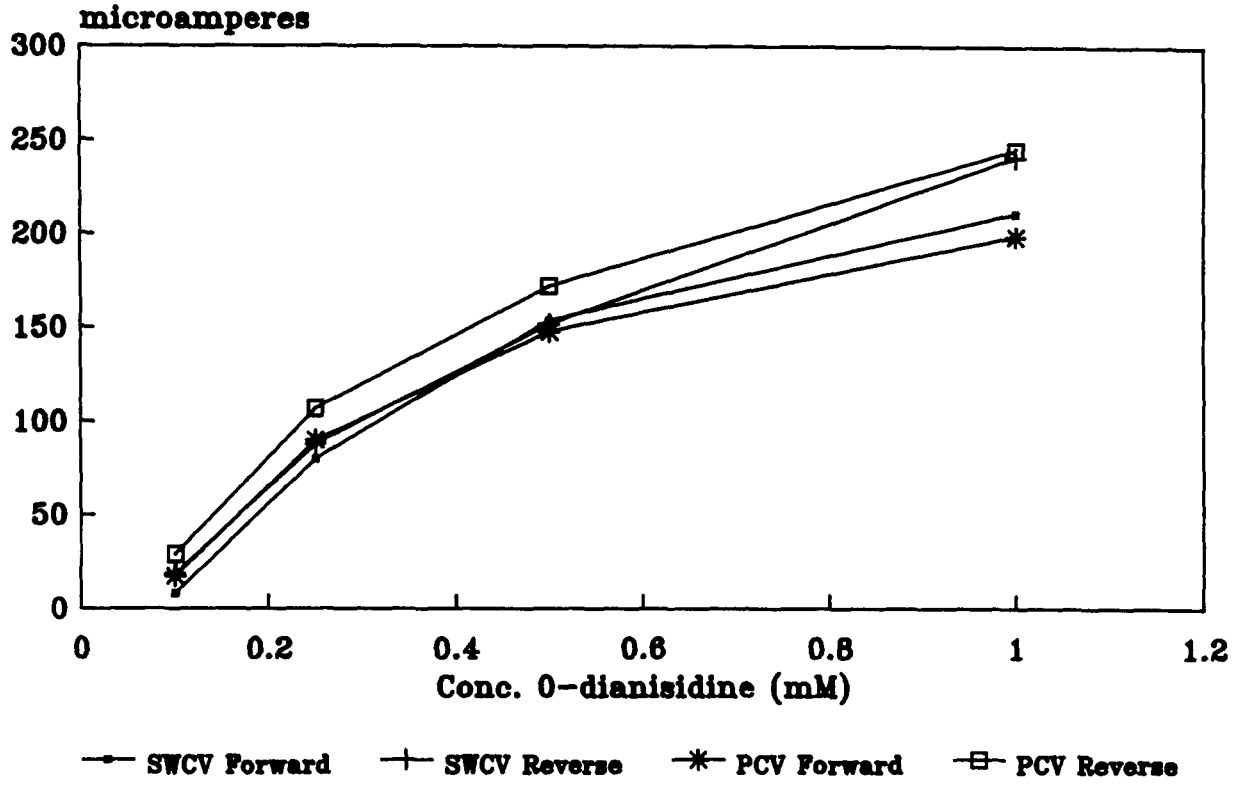

FIGURE 22. Difference current response for various concentrations of *O*-dianisidine. Number of cycles, 1; data acquisition frequency, 100 Hz; square-wave frequency, 50 Hz; square-wave amplitude, 66 mV; voltage ramp, 366 mV/s.

for the former technique was developed by Anderson and Reilley in the mid 1960s.[68] Weber and Purdy[66] suggested its use as an HPLC detector, and McClintock and Purdy[69,70] built an instrument and applied the technique to the analysis of catecholamines. It was found that the sensitivity increased as the flow rate decreased, compared to conventional single-working electrode electrochemical detectors.

Conventional amperometric detectors are operated at constant potentials determined from hydrodynamic voltammograms.[63] The high sensitivity of these detectors stimulated considerable interest; however, poor selectivity for poorly resolved chromatographic components was an early drawback. Methods to alleviate these problems have been proposed,[61,71] including the use of dual-working electrodes. Pulse techniques and rapid-scan techniques may overcome selectivity drawbacks, as outlined in the following section.

B. Pulse and Rapid-Scan Detectors in Flowing Streams

Pulse train detectors, as presented by Swartzfager[72] and reviewed by Kissinger[63] have been shown to offer increased selectivity and flow-rate independence. Some loss in sensitivity is sacrificed for increased selectivity. The flow-rate independence of these detectors was evaluated by Myers and Osteryoung[33] using normal and differential pulse techniques at rotated electrodes; they observed flow-rate independence when the Nernst layer thickness is small in comparison to the convective shear layer thickness, an important consideration when using solid electrodes in laminar flowing solutions.

Scanning a voltage range has the advantage of extending the selectivity characteristics of a detector. Consider a hypothetical representation of a two-dimensional current vs. time plot ob-

tained with a conventional amperometric electrochemical detector providing two distinct peaks (Figure 23). With a rapid scanning detector, an additional dimension is added by scanning the potential. The three-dimensional plot in Figure 24 indicates that peaks 1 and 2 (of Figure 23) are resolved on both the time axis and the potential axes, while peaks 1 and 3, unobserved on the time axis, are resolved from peak 1 on the potential axis. This illustrates the unique advantage of a scanning detector — its ability to electrochemically resolve species which are not resolved chromatographically.

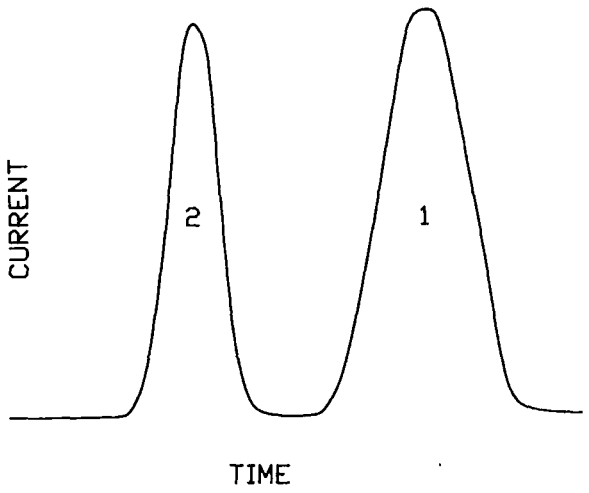

FIGURE 23. Representation of a current vs. time plot for an amperometric detector used in flowing streams.

Samuelsson et al.[73,74] used a static mercury drop electrode cell and studied both voltammetric detection and rapid-scan square-wave voltammetric detection of *N*-nitrosamines. Detection limits of approximately 10^{-7} *M* were obtained by both methods. The peak potentials offered qualitative information which can be used to aid the identification of unknown analytes. A subsequent article by the Osteryoungs summarized the results of this and related work.[75] A flow-through detector based on square-wave polarography at a dropping mercury electrode was evaluated by Wang et al.[76] and Scanlon et al.,[77] using the square-wave sweep potential method (dropping mercury electrode) for the three-dimensional detection of nitrophenols.

A solid electrode (glassy carbon) detector was developed by Stastny et al.[78] which utilized a double-pulse train and semidifferential evaluation of the single-sweep voltammogram during the chromatographic run. This detector was used to demonstrate the advantages of pulse techniques, compared with direct current ampometry, in terms of sensitivity and detection limits. The detection limit of picric acid using the pulse method (0.4 μg/l) was lower than that obtained with the amperometric detector (2.3 μg/l) (believed to be due to the variable "cleaning" potential used between successive pulses).

C. Considerations of a Pulse or Square-Wave Cyclic Voltammetric HPLC Detector

Cyclic alternating-current (AC) voltammetry has been discussed in detail by Bond and coworkers,[79,80] covering both theory and experimental results for electrode reactions involving solution redox couples and amalgam formation. It was concluded that fundamental and second-harmonic AC cyclic voltammograms complement DC CV, and can provide more sensitivity and convenient insights into the electrode reaction. This technique should be useful as an electrochemical detector in HPLC; however, sophisticated auxiliary equipment (e.g., lock-in amplifiers) is needed.

Before a decision is made in choosing a particular detector configuration, a general review of detection requirements is recommended. Amperometric detectors for liquid chromatography are in widespread use for the trace determination of easily oxidized organic compounds. Recent technological advances and applications in this area have been reviewed and should be examined. Easily reducible compounds received little attention until sufficient advances were made in preparing a reliable mercury electrode.[81] Another limitation has been the need to remove oxygen in order to reduce background current levels. Various techniques for eliminating oxygen have been developed, but they can serve to increase the complexity of the instrumentation.[81-83] An additional problem is the reduction of trace metals at negative potentials, which decreases the current response by reducing the effective area of

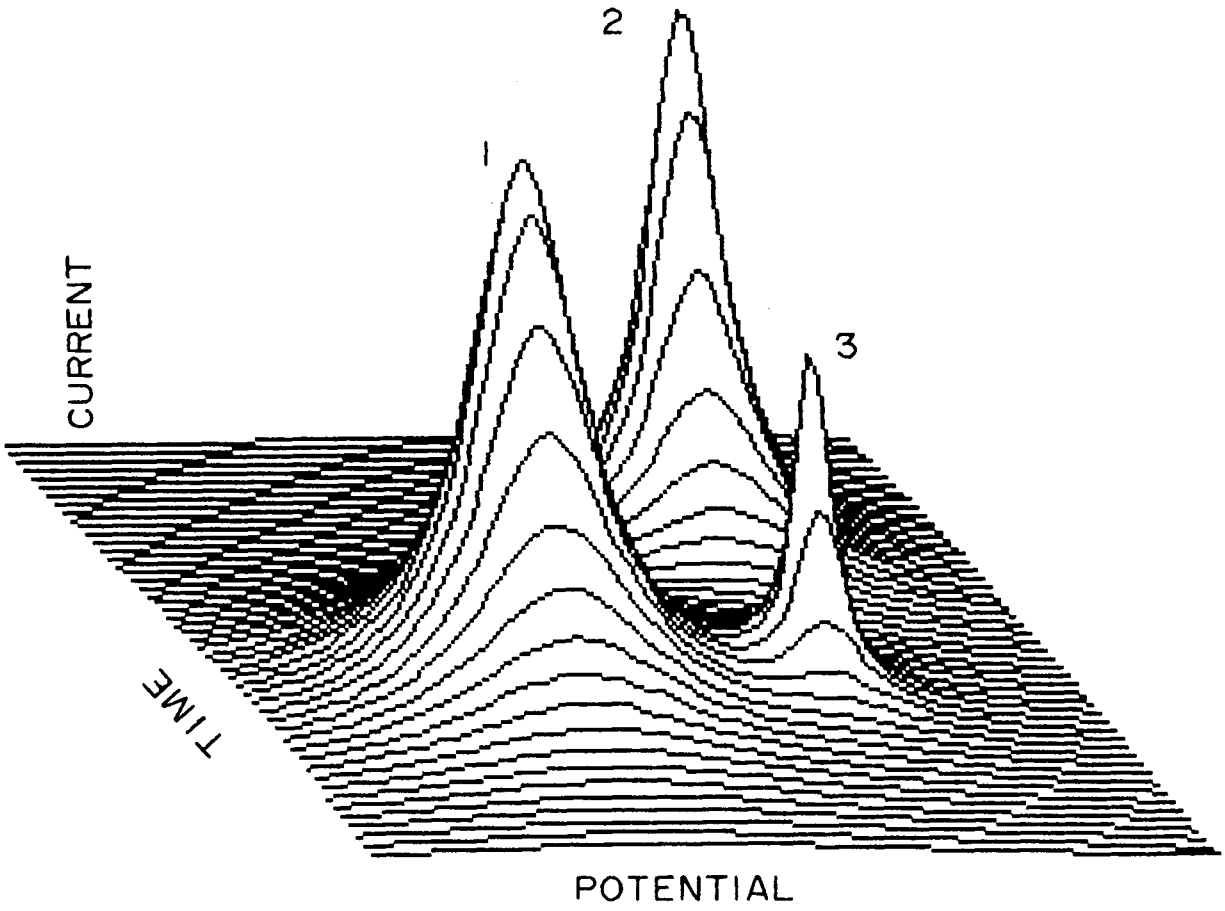

FIGURE 24. Representation of a three-dimensional plot for a rapid-scan detector used in flowing streams.

the electrode. In such cases, electrode "clean-up" procedure is usually necessary. In this regard, an advantage of the dropping mercury electrode is its renewable surface, this, coupled with its high hydrogen overpotential, has made this electrode perhaps the most widely used and studied for electrochemical detection.

Glassy carbon and carbon paste electrochemical detectors are commercially available, and recent advances indicate that other types will undoubtedly appear on the market.[61,62] Low-temperature isotropic carbon (LTIC) has the largest potential window in aqueous solutions among he common solid electrode materials (+1.39 to −1.43 V),[84] making it the most versatile electrode material available in terms of detecting compounds that are easily oxidized or reduced. Another useful property of LTIC is its ability to be polished to a microscopically flat, uniform appearance. There are two important features to be considered in an electrochemical reaction: the electrochemical reaction rate and the rate of mass transport. The electrode area and the thickness of the cell in an electrochemical HPLC detector can be optimized for high mass-transport efficiency.[66] The electrochemical reaction rate, on the other hand, is a function determined by the electrode material and the reactive species in solution. It has been shown that the LTIC electrode exhibits faster kinetics for some compounds, relative to carbon paste, but the opposite is true for others.[84]

Rapid-scanning electrochemical detection for HPLC or FIA[84] has been investigated with channel-type electrochemical flow cells which utilize glassy carbon and carbon fibers as working electrode materials. A cyclic voltammetric staircase waveform has been employed for an FIA system based on a two-electrode detection method in which the working electrode consisted of a car-

bon fiber microelectrode.[85] FIA and CV were investigated by Thogersen et al.,[86] who found that less time was necessary to obtain diagnostic information using CV than obtaining a hydrodynamic voltammogram under the same conditions.

The problem of electrode-fouling effects on the electrode surface caused by adsorption of products of analyte reduction was found to be minimized in the square-wave detection mode.[81] Other methods such as electrochemical stripping and the use of a differential pulse mode have also been shown to be useful for reducing electrode fouling.[78,87]

One can calculate that, in an HPLC electrochemical detector with a cell volume of 1 μl and a flow rate of 1 ml/min, it would take 0.06 s for a molecule to traverse the active surface. To obtain electrochemical information from such a molecule using a rapid-scan technique, it is evident that the scan must be completed well within the same time interval. If it is assumed that a pulse CV utilizing a 2-V (−0.5 to +0.5 and back to −0.5 V) scan is obtainable, then for a 0.06-s time restriction, the minimum scan rate required is 33 V/s. This restricts detection to relatively rapid electron transfer processes. If the cell volume was increased to 10 μl and the flow rate reduced to 0.5 ml/min, then a scan rate of 1.7 V/s would be required to cover the same voltage window. This shows that there is some flexibility available, considering a flow rate of 0.5 ml/min does not alter the chromatographic analysis time significantly, and a flow cell of 10 μl is simple to build. Although the detector resolution and sensitivity are affected by these variables, the square-wave technique offers additional control since the pulse amplitude and frequency can be varied as shown by studies at the mercury electrode.[44,75])

D. Effect of the Transfer Coefficient on Voltammogram Symmetry in Flowing Solutions

The purpose here is to show that the conclusions that were drawn in Section IV for static solution studies can, using FIA, be extended to flowing solutions. Thogersen et al.[86] suggested the power of combining CV with FIA, utilizing the diagnostic power of the former and the flexibility of the latter. Eccles and Purdy[51] combined PCV with FIA, and Figure 25 is redrawn from their studies (n.b., the series of scans have been arbitrarily spaced apart for clarity). In the upper cathodic scans, a peak representing the reduction of hydroquinone to quinone is observed (peak potential, 0.249 V vs. Ag/AgCl). The lower oxidation (hydroquinone to quinone) peak is better defined ($\alpha = 0.32$) than the reduction peak (peak potential, 0.393 V vs. Ag/AgCl). Figure 26 (redrawn data from Reference 51) shows four peaks (as did the static solution study; see Figure 19). Again, the forward and reverse scans are arbitrarily spaced apart for clarity (peak potentials for the upper reduction peaks, left to right, are 0.314 and 0.332 V Ag/AgCl, and for the lower oxidation peaks, left to right, are 0.499 and 0.470 V vs. the same reference electrode). The difference plot (Figure 27) of the data in Figure 26 shows two peaks (left peak: the total current from the forward scans; right peak: the total current from the reverse scans). The forward and reverse scan peak potentials were 0.396 and 0.404 V, respectively, vs. Ag/AgCl. The oxidation peak (peak on right) in Figure 27 (consistent with static solution case in Figure 20) predominates, indicating the reversibility of the couple. These results indicate, that for an injected sample of quinone, the oxidation current during the long time scale provides better analytical sensitivity. This also suggests the analytical utility of PCV or SWCV detection.

The diagnostic information provided above for flowing solutions compares favorably with that obtained from static solution studies, indicating its suitability in determining the potentials of interest for conventional DC amperometric detection. One distinct advantage of these detectors is their high sensitivity for electrochemically active compounds. It is advantageous to collect such diagnostic information under the same conditions in which the DC amperometric detector will be operated. After the required information is obtained, the scanning detector can function as a DC amperometric detector by setting it to the appropriate potential.

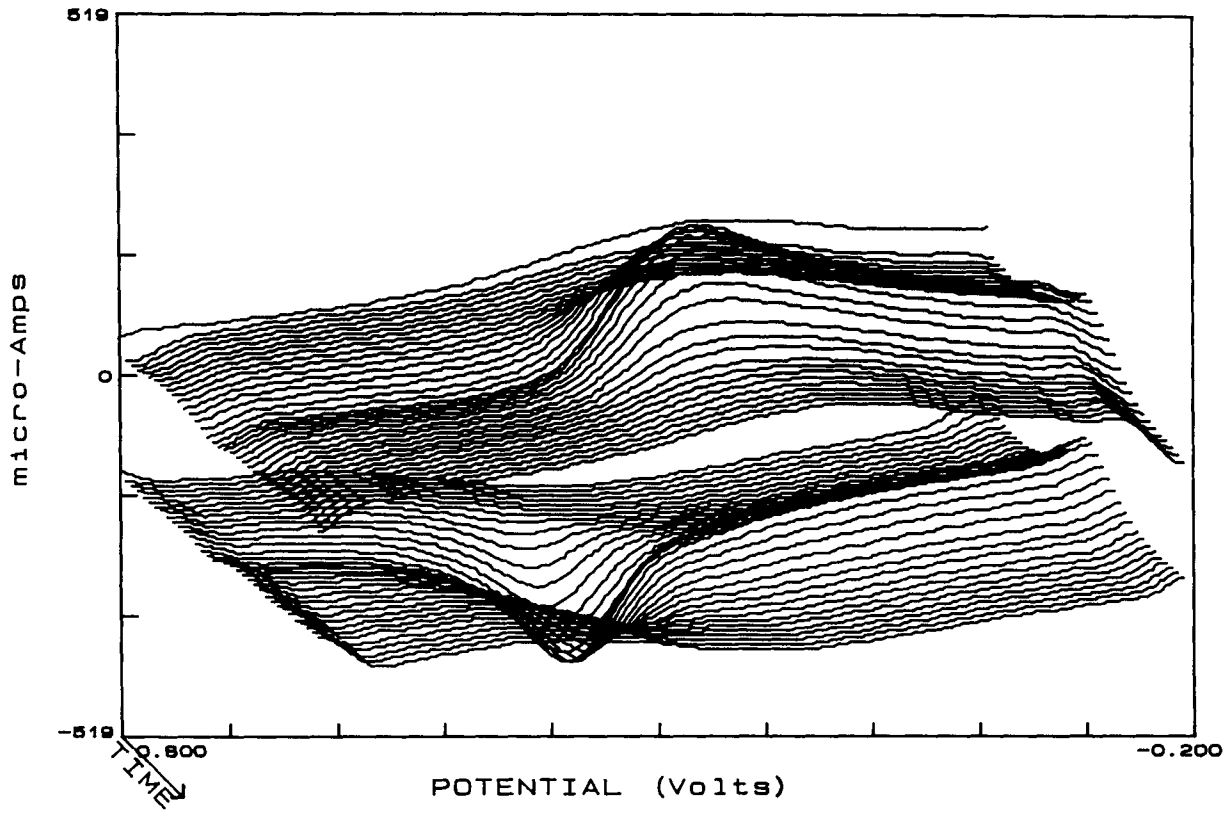

FIGURE 25. Fourier-smoothed cyclic chronovoltammogram of 1 m*M* quinone in 1 *M* sulfuric acid. Initial time delay, 35 s; number of cycles, 35; data acquisition frequency, 120 Hz; voltage ramp, 1 V/s.

E. Quantitative Study in Flowing Streams Using PCV and FIA

Eccles and Purdy[51] investigated the feasibility of quantitative determinations with LTIC, using PCV and FIA with the ferri-ferrocyanide couple. To illustrate, Figure 28 shows the presence of two peaks: the major reduction currents obtained during the negative scans are shown on the left side of the switching potential, the major oxidation currents, on the right. The signal can be enhanced up to a factor of ten by integrating the pulse cyclic chronovoltammogram with respect to the time axis for those cycles containing a response (see Figure 29a). This plot is a total signal current-response curve containing significant high-frequency noise; after Fourier smoothing, the noise is reduced considerably and the peak currents can be easily measured (see Figure 29b).

The same investigators[50,51] also showed that the detection limits improved when using a PCV waveform instead of a CV waveform. In CV, they obtained a detection limit of 1×10^{-5} *M* for ferricyanide in static solution. With PCV in static solution, the detection limit improved to 0.4×10^{-5}, while in a flowing stream, a value of 0.2×10^{-5} was measured. The advantage of the flowing stream detection method is that a smaller sample is required and background correction may be achieved by using one of the cycles prior to peak elution.

F. Analysis of Mixture Using PCV and FIA

Figure 30 shows the reaction similarity between quinone/hydroquinone (in b) (treated previously) and menadione (in a). The latter has the same electroactive group and should offer the same redox behavior. Studies were made of mixtures of quinone and menadione in an FIA system using SWCV.[88] Figure 31 shows the results ob-

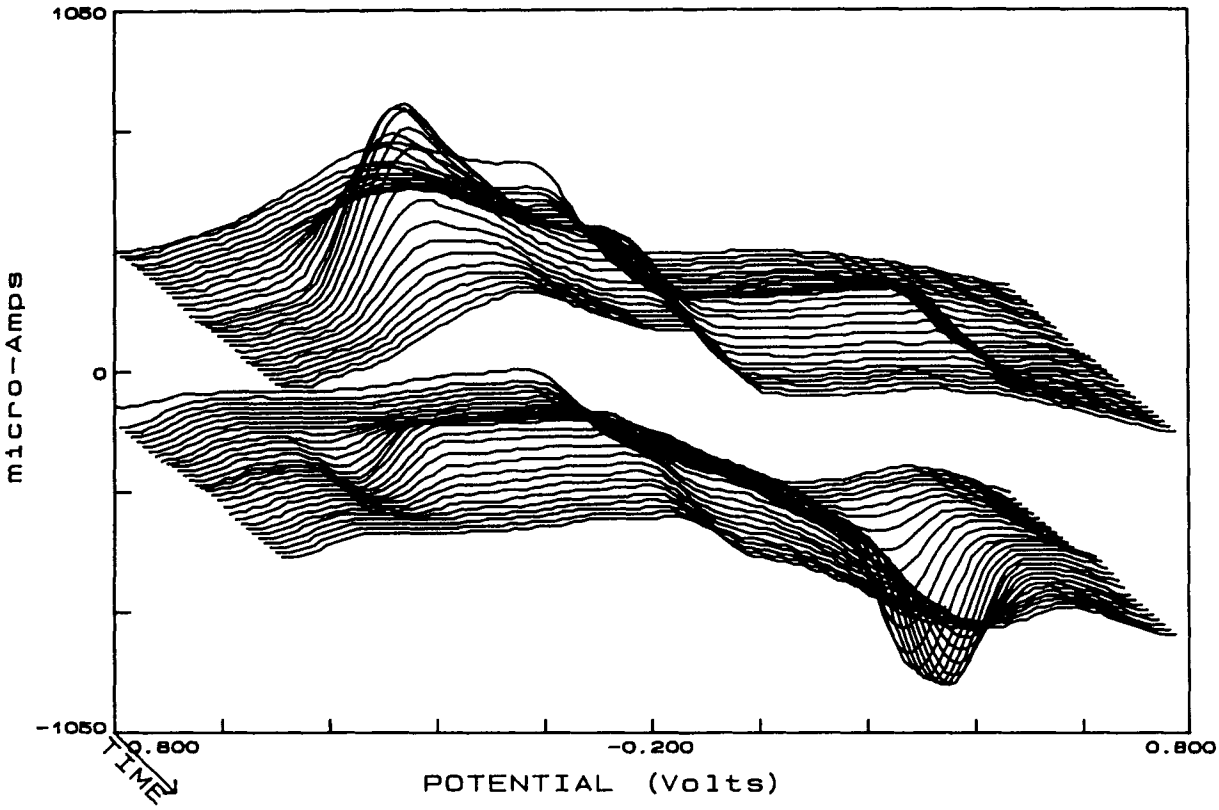

FIGURE 26. Fourier-smoothed pulse cyclic chronovoltammogram of 1 m*M* quinone in 1 *M* sulfuric acid. Initial time delay, 35 s; number of cycles, 30; data acquisition frequency, 120 Hz; square-wave frequency, 60 Hz; voltage ramp, 1 V/s.

tained for a solution of 1 m*M* menadione in a 20% mixture of acetonitrile in 1 *M* H_2SO_4. On the left are the positive scan data (oxidation peak potential, 0.100 V vs. Ag/AgCl); on the right, the negative scan data (reduction peak potential, 0.018 V vs. Ag/AgCl). The results indicate that diagnostic information can be obtained from the modified waveforms, considering the direction in which the forward scan was initiated. Usually, when CV is performed, the forward scan direction is implemented as a reduction or oxidation, depending on the electrochemistry involved. For menadione, it was expected that the forward scan direction should have been negative; in contrast (Figure 31), a positive scan was initiated, indicating that this technique is not susceptible to the oxidation state of the starting material for redox couples. This is an asset not to be overlooked since it eliminates the interpretation of the oxidation state of the starting material.

The examination of a mixture of quinone and menadione (Figure 32) produced four peaks: the two on the left of the switching potential are completely resolved on the potential axis, while the two on the right are not. However, by plotting cycles 14 and 15, the peaks are more easily discernable (Figure 33); peak potentials, left to right: 0.100, 0.544, 0.018, and −0.271 V, vs. Ag/AgCl. From these potentials, the electron transfers for menadione are represented (left to right) by peaks 1 and 3; those for quinone are represented by peaks 2 and 4 (note that peak 3 is smaller than peak 1). The large separation for the quinone/hydroquinone couple has not been investigated, but may be due to the addition of acetonitrile.

VI. CONCLUSIONS

As an analytical utility PCV and SWCV have much to offer, both qualitatively and quantitatively. The methods available for displaying the data of the dual-time techniques offer distinct advantages in the interpretation of results. For

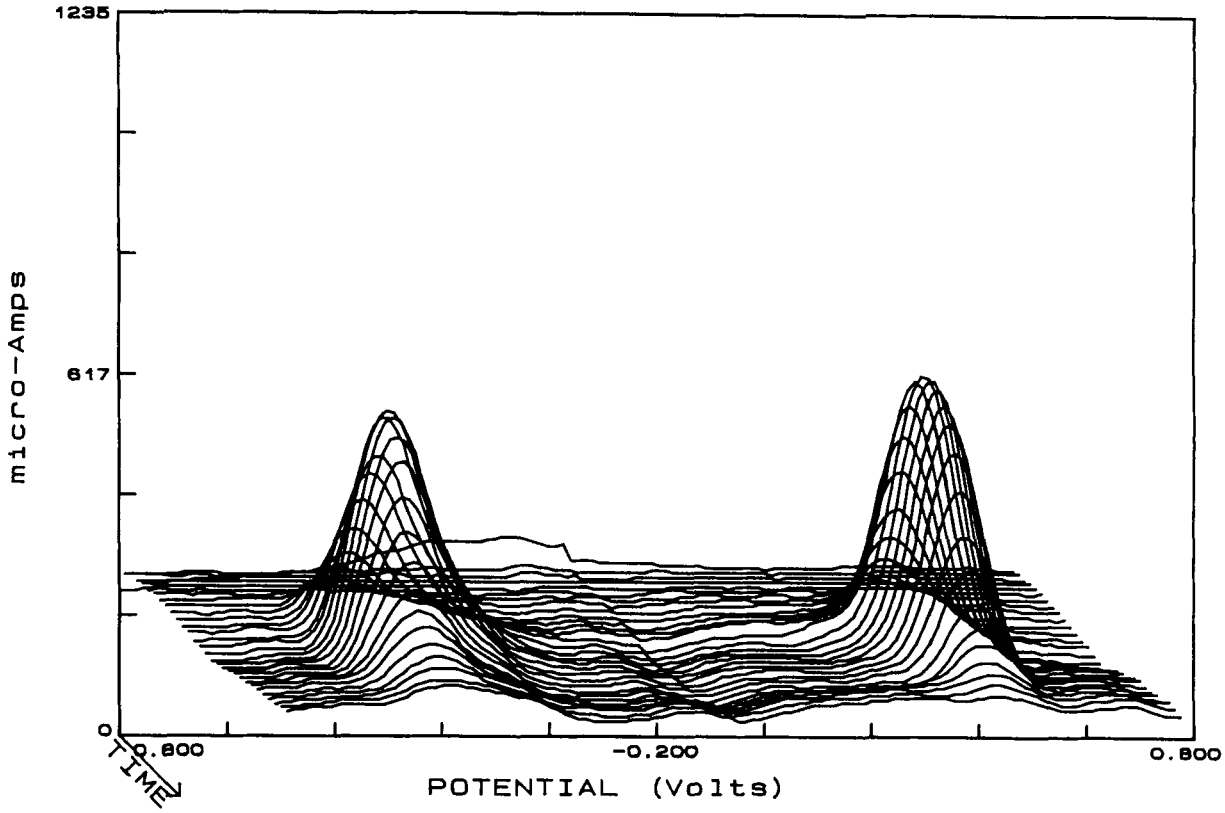

FIGURE 27. Fourier-smoothed, background-corrected, absolute-difference plot obtained from the data in Figure 26.

example, the difference current plots considerably simplify the determination of peak heights and peak positions along the potential axis. On the other hand, the pulse currents offer insights into electrode processes of a more qualitative nature. The advantage of the SWCV waveform is the transition and hold potential during a pulse, which offers an increase in sensitivity. For the higher-capacitance carbon electrodes, the PCV waveforms offer the advantage that pulse transitions are symmetric, and difference-current response curves can provide unbiased background corrections.

The electrode itself, plays a significant role in the performance of any electroanalytical technique. With the advent of microelectrodes[89] and microarrays,[90] capacitive charging currents — the limiting factor in transient techniques — are reduced significantly. The rate of mass transport between the electrode and the solution, an important factor in electrochemical reactions, increases as the electrode size decreases. In addition, it has been shown that rapid scanning techniques at microelectrodes can be used in highly resistive solutions.[91]

In summation, then, CV offers a diverse arsenal of diagnostic methods to study, evaluate, and quantify electrochemical and (indirectly) nonelectrochemical processes occurring at or near electrode surfaces. With further research, PCV and SWCV should become even more attractive and more valuable analytical extensions to CV.

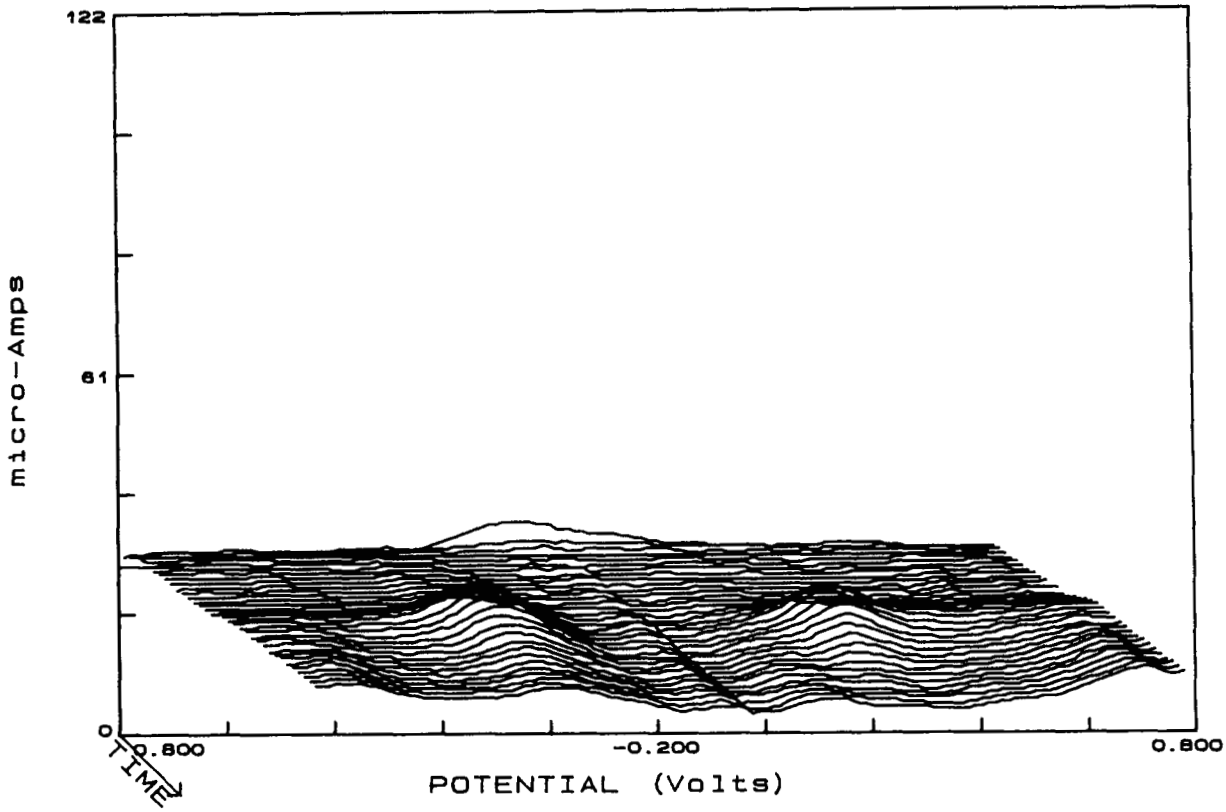

FIGURE 28. Background-corrected, absolute PCV difference plot of 0.08 m*M* ferricyanide in 1 *M* sulfuric acid. Initial time delay, 35 s; number of cycles, 35; data acquisition frequency, 130 Hz; square-wave frequency, 65 Hz; square-wave amplitude, 100 mV; voltage ramp, 1 V/s.

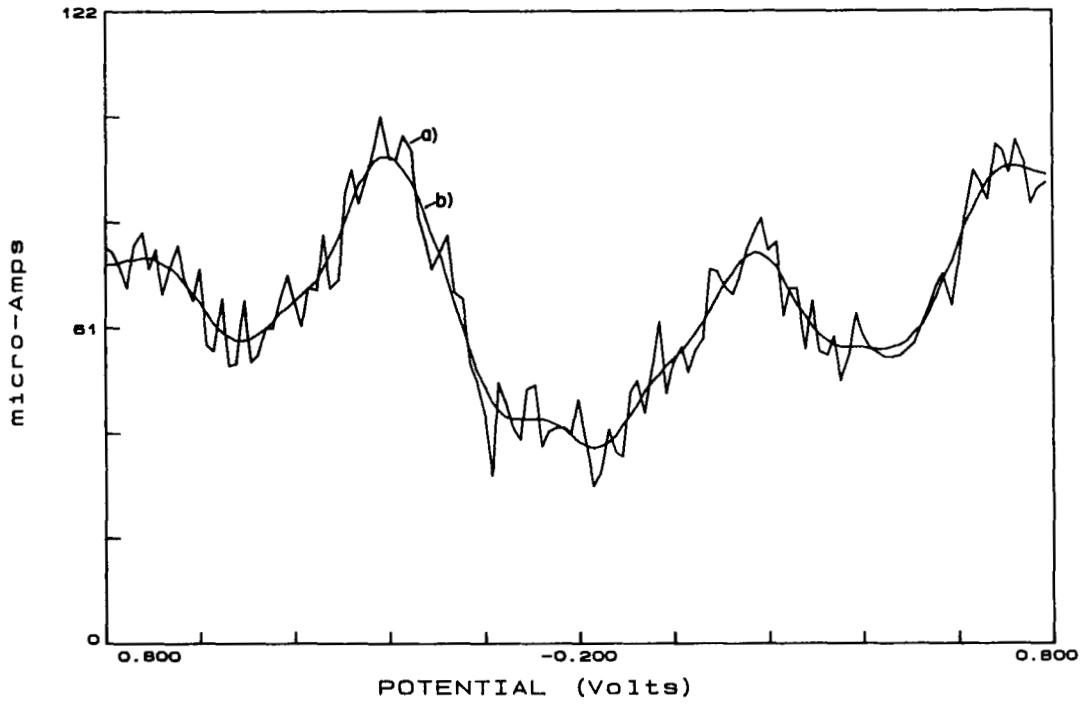

FIGURE 29. Time-integrated plot of Figure 28. (a) Before Fourier smoothing; (b) after Fourier smoothing.

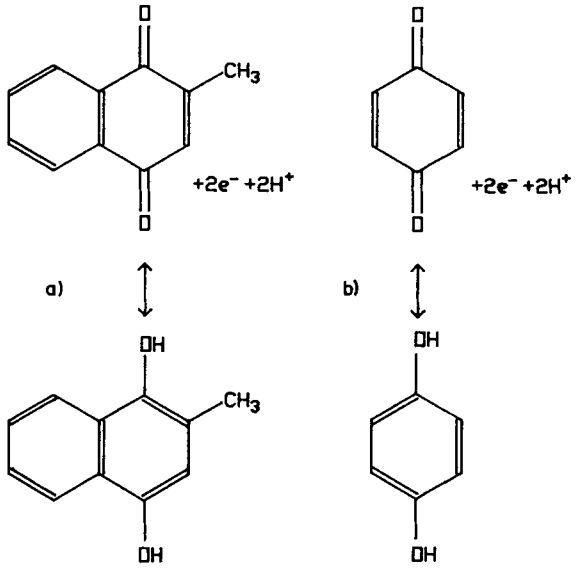

FIGURE 30. Redox reactions for (a) menadione and (b) quinone.

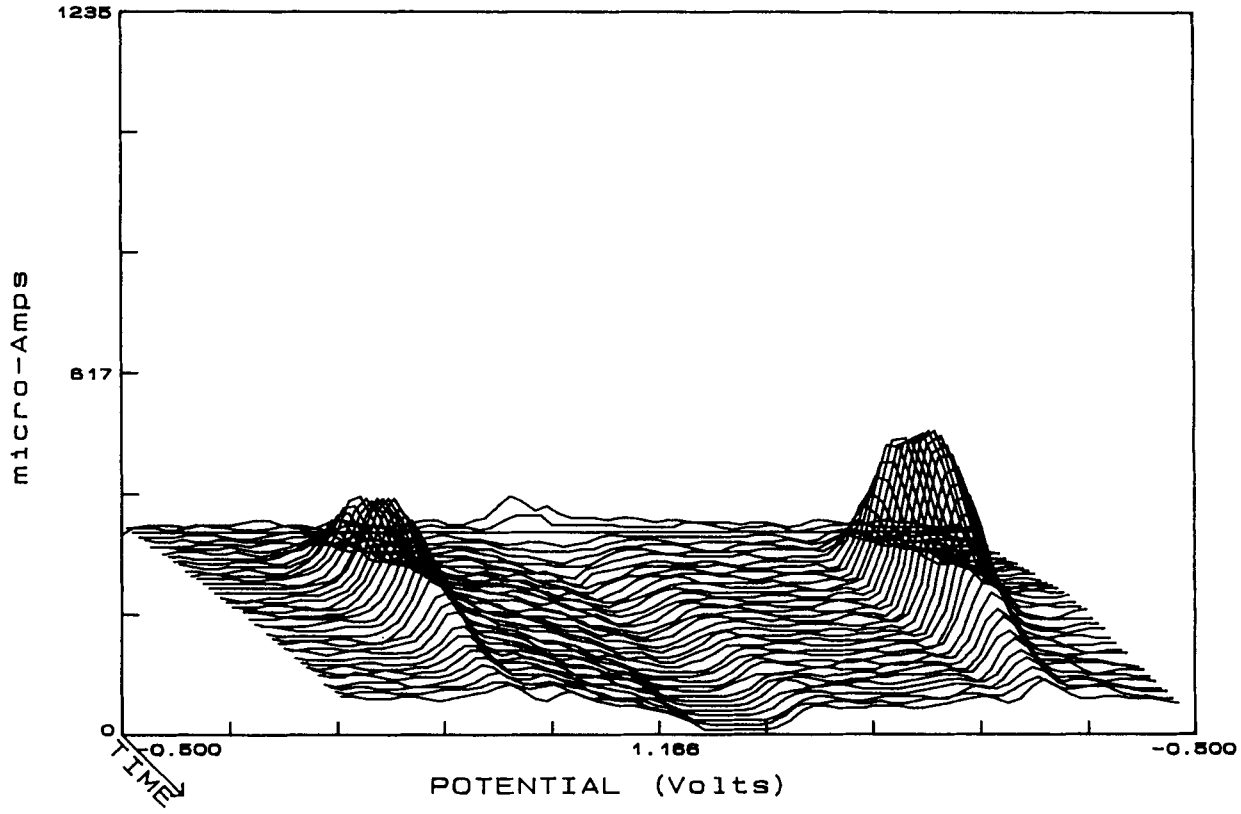

FIGURE 31. Fourier-smoothed, background-corrected SWCV difference chronovoltammogram of 1 m*M* menadione in 20% acetonitrile in 1*M* sulfuric acid. Initial time delay, 40 s; flow rate, 0.150 ml/min; number of cycles, 40; data acquisition frequency, 70 Hz; square-wave frequency, 35 Hz; square wave amplitude, 100 mV; voltage ramp, 1.67 V/s.

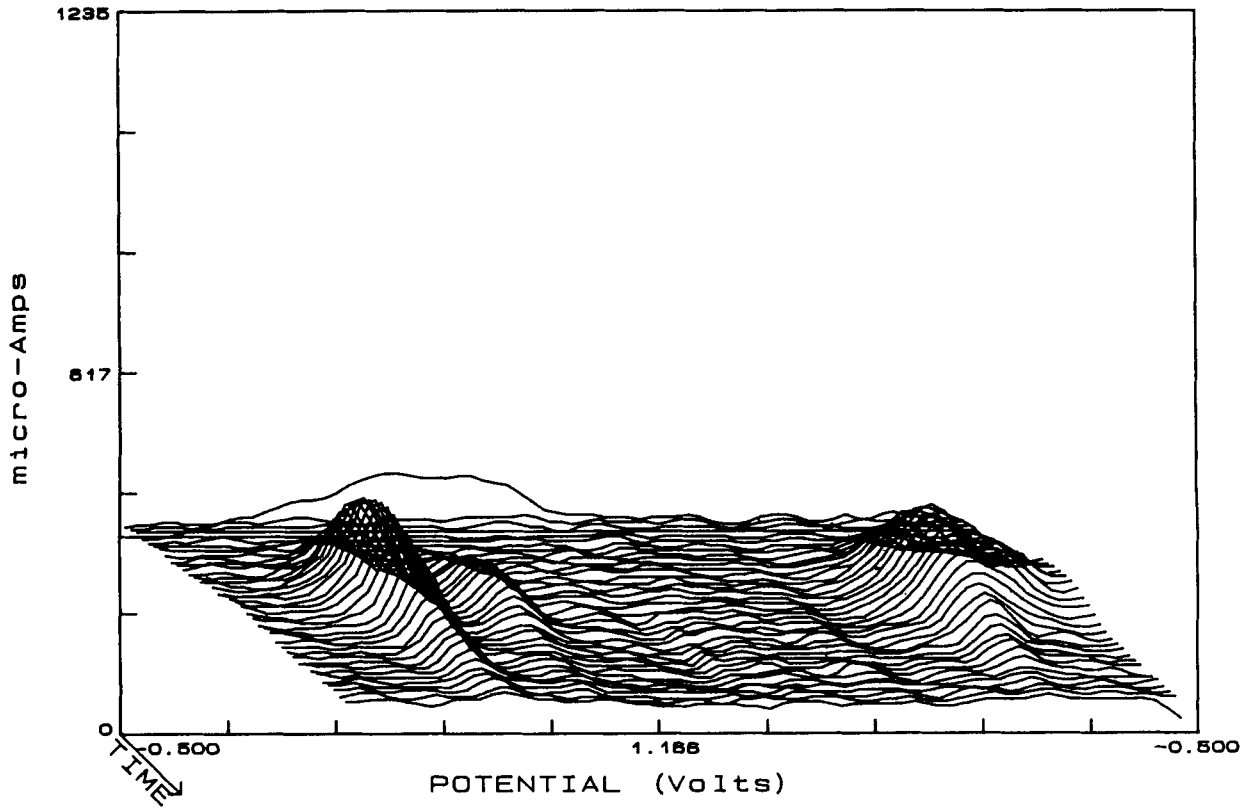

FIGURE 32. Fourier-smoothed, background-corrected SWCV difference chronovoltammogram of 1 m*M* menadione and 1 m*M* quinone in 20% acetonitrile in 1 *M* sulfuric acid. Initial time delay, 40s; flow rate, 0.150 ml/min; number of cycles, 40; data acquisition frequency, 70 Hz; square-wave frequency, 35 Hz; square wave amplitude, 100 mV; voltage ramp, 1.67 V/s.

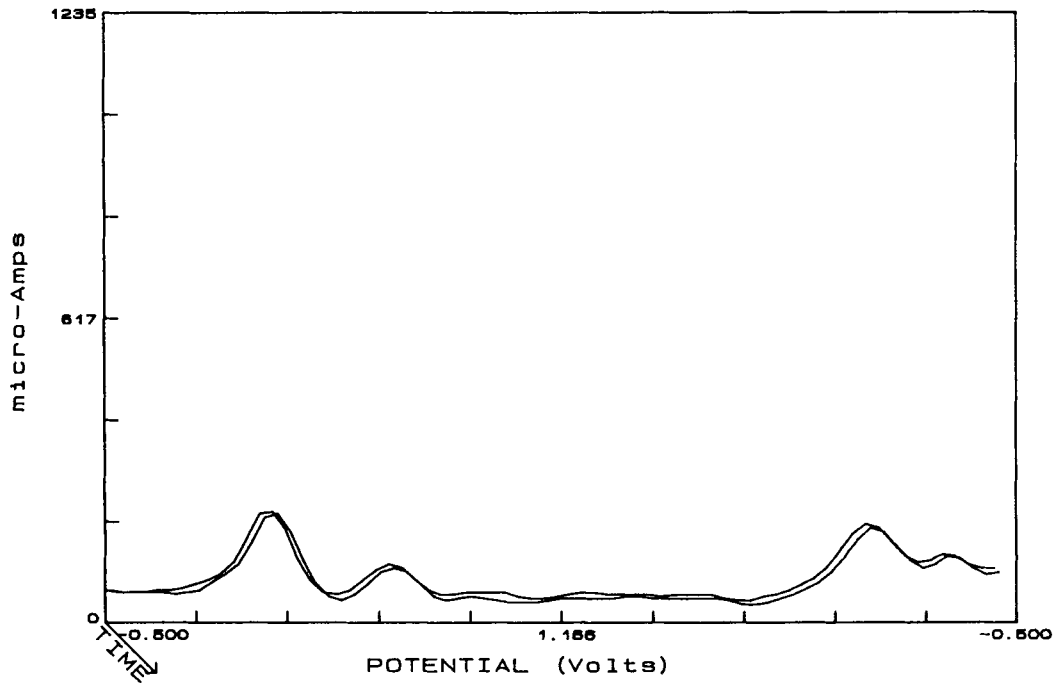

FIGURE 33. Plot of cycles 14 and 15 in Figure 32.

REFERENCES

1. **Adams, R. N.,** *Electrochemistry at Solid Electrodes,* Marcel Dekker, New York, 1969, 143.
2. **Kissinger, P. T. and Heineman, W. R.,** *J. Chem. Ed.,* 60, 702, 1983.
3. **Mabbott, G. A.,** *J. Chem. Ed.,* 60, 697, 1983.
4. **Nicholson, R. S. and Shain, I.,** *Anal. Chem.,* 36, 706, 1964.
5. **Nicholson, R. S.,** *Anal. Chem.,* 37, 667, 1965.
6. **Bard, A. J. and Faulkner, L. R.,** *Electrochemical Methods: Fundamentals and Applications,* John Wiley & Sons, New York, 1980, 442.
7. **Kissinger, P. T. and Heineman, W. R., Eds.,** *Laboratory Techniques in Electroanalytical Chemistry,* Marcel Dekker, New York, 1984, 82.
8. **Kemula, W. and Kublik, Z.,** *Nature,* 182, 793, 1958.
9. **Powers, M. J. and Meyers, T. J.,** *J. Am. Chem. Soc.,* 102, 1289, 1980.
10. **Rice, C. A. and Spence, J. T.,** *Inorg. Chem.,* 19, 2845, 1980.
11. **Bobbitt, J. M. and Wills, J. P.,** *J. Org. Chem.,* 45, 1978, 1980.
12. **Nelson, S. F., Kessel, C. R., Brien, D. J., and Weinhold, F.,** *J. Org. Chem.,* 45, 2116, 1980.
13. **Sevcik, A.,** *Collect. Czech. Chem. Commun.,* 13, 349, 1948.
14. **Creason, S. C., Loyd, R. J., and Smith, D. E.,** *Anal. Chem.,* 44, 1159, 1972.
15. **Heyrovsky, J.,** *Analyst,* 72, 229, 1947.
16. **Grahame, D. C.,** *J. Am. Chem.,* 71, 2975, 1949.
17. **Bard, A. J. and Faulkner, L. R.,** *Electrochemical Methods: Fundamentals and Applications,* John Wiley & Sons, New York, 1980, chap. 9.
18. **Kissinger, P. T. and Heineman, W. R., Eds.,** *Laboratory Techniques in Electroanalytical Chemistry,* Marcel Dekker, New York, 1984, 151.
19. **Barker, G. C. and Jenkins, I. J.,** *Analyst,* 77, 685, 1952.
20. **Barker, G. C.,** *Anal. Chim. Acta,* 18, 118A, 1958.
21. **Barker, G. C. and Gardner, A. W.,** *Z. Anal. Chem.,* 173, 79, 1960.
22. **Barker, G. C., Gardner, A. W., and Williams, M. J.,** *J. Electroanal. Chem.,* 42, App. 21, 1973.
23. **Kissinger, P. T. and Heineman, W. R., Eds.,** *Laboratory Techniques in Electroanalytical Chemistry,* Marcel Dekker, New York, 1984, 500.
24. **Bard, A. J. and Faulkner, L. R.,** *Electrochemical Methods: Fundamentals and Applications,* John Wiley & Sons, New York, 1980, p. 143.
25. **Brinkman, A. A. A. M. and Los, J. M.,** *J. Electroanal. Chem.,* 14, 269, 1967.
26. **Brinkman, A. A. A. M. and Los, J. M.,** *J. Electroanal. Chem.,* 14, 285, 1967.
27. **Brinkman, A. A. A. M. and Los, J. M.,** *J. Electroanal. Chem.,* 7, 171, 1964.
28. **Parry, E. P. and Osteryoung, R. A.,** *Anal. Chem.,* 36, 1366, 1964.
29. **Parry, E. P. and Osteryoung, R. A.,** *Anal. Chem.,* 37, 1634, 1965.
30. **Christie, J. H. and Osteryoung, R. A.,** *J. Electroanal. Chem.,* 49, 301, 1974.
31. **Christie, J. H., Jackson, L. L., and Osteryoung, R. A.,** *Anal. Chem.,* 48, 242, 1976.
32. **Brumleve, T. R., O'Dea, J. J., Osteryoung, R. A., and Osteryoung, J.,** *Anal. Chem.,* 53, 702, 1981.
33. **Myers, D. J. and Osteryoung, R. A.,** *Anal. Chem.,* 46, 2089, 1974.
34. **Blutstein, H. and Bond, A. M.,** *Anal. Chem.,* 48, 248, 1976.
35. **Osteryoung, J. and Hasebe, K.,** *Rev. Polarogr., (Jpn.), 22, 1, 1976.*
36. **Kemula, W. and Kublik, Z.,** *Rocz. Chem.,* 30, 1005, 1956.
37. **Christie, J. H. and Osteryoung, R.,** *Anal. Chem.,* 48, 869, 1976.
38. **Oldham, K. B.,** *Trans. Faraday Soc.,* 53, 80, 1957.
39. **Christie, J. H., Turner, J. A., and Osteryoung, R. A.,** *Anal. Chem.,* 49, 1899, 1977.
40. **Turner, J. A., Christie, J. H., Vukovic, M., and Osteryoung, R. A.,** *Anal. Chem.,* 49, 1904, 1977.
41. **Osteryoung, R. A. and Osteryoung, J.,** *Philos. Trans. R. Soc. London Ser. A,* 302, 315, 1981.
42. **Bard, A. J., Ed.,** *Electroanalytic Chemistry,* Marcel Dekker, New York, 1986, 209.
43. **Krause, M. S., Jr. and Ramaley, L.,** *Anal. Chem.,* 41, 1365, 1969.
44. **Christie, J. H. and Lingane, P. J.,** *J. Electroanal. Chem.,* 10, 176, 1965.
45. **Drake, K. F., VanDuyne, R. P., and Bond, A. M.,** *J. Electroanal. Chem.,* 89, 231, 1978.
46. **Okamoto, K.,** *Rev. Polarogr. Jpn.,* 12, 40, 1964.
47. **Gajda, V. and Horák, K.,** *Anal. Chim. Acta,* 134, 219, 1982.
48. **Ramaley, L. and Tan, W. T.,** *Can. J. Chem.,* 65, 1025, 1987.
49. **Eccles, G. N. and Purdy, W. C.,** *Anal. Lett.,* 18, 657, 1985.
50. **Eccles, G. N. and Purdy, W. C.,** *Can. J. Chem.,* 65, 1051, 1987.
51. **Eccles, G. N. and Purdy, W. C.,** *Can. J. Chem.,* 65, 1795, 1987.
52. **Kissinger, P. T. and Heineman, W. R., Eds.,** *Laboratory Techniques in Electroanalytical Chemistry,* Marcel Dekker, New York, 1984, 195.
53. **Adams, R. N.,** *Electrochemistry at Solid Electrodes,* Marcel Dekker, New York, 1969, 37.
54. **Adams, R. N.,** *Electrochemistry at Solid Electrodes,* Marcel Dekker, New York, 1969, 135.
55. **Nicholson, R. S. and Shain, I.,** *Anal. Chem.,* 36, 1964 (Table III).
56. **Eccles, G. N.,** Ph.D. thesis, McGill University, Montreal, 1988, 161.
57. **Nicholson, R. S.,** *Anal. Chem.,* 37, 1351, 1965.
58. **Eccles, G. N.,** Ph.D. thesis, McGill University, Montreal, 1988, 171.
59. **Kissinger, P. T., Refshauge, C., Dreiling, R., and Adams, R. N.,** *Anal. Lett.,* 6, 465, 1973.

60. **Anon.,** LC for Problem Solvers, Bioanalytical Systems (flyer), October 1982.
61. **Roston, D. A., Shoup, R. E., and Kissinger, P. T.,** *Anal. Chem.*, 54, 1417A, 1982.
62. **McClintock, S. A. and Purdy, W. C.,** *Int. Lab.*, 14(7), 70, 1984.
63. **Kissinger, P. T.,** *Anal. Chem.*, 49, 447A, 1977.
64. **Weber, S. G. and Purdy, W. C.,** *Ind. Eng. Chem. Prod. Res. Dev.*, 20, 593, 1981.
65. **Matsuda, H.,** *J. Electroanal. Chem.*, 15, 325, 1967.
66. **Weber, S. G. and Purdy, W. C.,** *Anal. Chim. Acta*, 100, 531, 1978.
67. Exhibition Floor Exhibitors, Bioanalytical Systems (BAS) and Princeton Applied Research (PAR), Pittsburgh Conference, New Orleans, 1985.
68. **Anderson, L. B. and Reilley, C. N.,** *J. Electroanal. Chem.*, 10, 295, 1965.
69. **McClintock, S. A. and Purdy, W. C.,** *Anal. Lett.*, 14, 791, 1981.
70. **McClintock, S. A. and Purdy, W. C.,** *Anal. Chim. Acta*, 148, 127, 1983.
71. **Blank, C. L.,** *J. Chromatogr.*, 117, 35, 1976.
72. **Swartzfager, D. G.,** *Anal. Chem.*, 48, 2189, 1976.
73. **Samuelsson, R., O'Dea, J., and Osteryoung, J.,** *Anal. Chem.*, 52, 2215, 1980.
74. **Samuelsson, R. and Osteryoung, J.,** *Anal. Chim. Acta*, 123, 97, 1981.
75. **Osteryoung, J. G. and Osteryoung, R. A.,** *Anal. Chem.*, 57, 101A, 1985.
76. **Wang, J., Ouzeil, E., Yarnitzky, Ch., and Ariel, M.,** *Anal. Chim. Acta*, 102, 99, 1978.
77. **Scanlon, J. J., Flaquer, P. A., Robinson, G. W., O'Brien, G. E., and Sturrock, P. T.,** *Anal. Chim. Acta*, 158, 169, 1984.
78. **Stastny, M., Volf, R., Benadikova, H., and Vit, I.,** *J. Chromatogr. Sci.*, 21, 18, 1983.
79. **Bond, A. M., O'Halloran, R. J., Ruzic, I., and Smith, D. E.,** *Anal. Chem.*, 48, 872, 1976.
80. **Bond, A. M., O'Halloran, R. J., and Smith, D. E.,** *Anal. Chem.*, 50, 216, 1978.
81. **Bratin, K. and Kissinger, P. T.,** *J. Liq. Chromatogr.*, 4(Suppl. 2), 321, 1981.
82. **Bratin, K. and Kissinger, P. T.,** *J. Liq. Chromatogr.*, 4, 1777, 1981.
83. **Hepler, B. R., Weber, S. G., and Purdy, W. C.,** *Anal. Chim. Acta*, 102, 41, 1978.
84. **Caudill, W. L., Ewing, A. G., Jones, S., and Wightman, R. M.,** *Anal. Chem.*, 55, 1877, 1983.
85. **White, J. G., St. Claire, R. L., III, and Jorgenson, J. W.,** *Anal. Chem.*, 58, 293, 1986.
86. **Thogersen, N., Janata, J., and Ruzicka, J.,** *Anal. Chem.*, 55, 1988, 1983.
87. **MacCrehan, W. A.,** *Anal. Chem.*, 53, 74, 1981.
88. **Eccles, G. N.,** Ph.D. thesis, McGill University, Montreal, 1988, 206.
89. **Pons, S. and Fleischman, M.,** *Anal. Chem.*, 59, 1391A, 1987.
90. **Weisshaar, D. E. and Tallman, D. E.,** *Anal. Chem.*, 55, 1146, 1983.
91. **Howell, J. O. and Wightman, R. M.,** *Anal. Chem.*, 56, 524, 1984.